TITLE

60S subunit joining exposes nascent pre-40S rRNA for quality control

AUTHORS

Jay Rai[1,2], Melissa D. Parker[2,3], Haina Huang[3], Stefan Choy[3], Homa Ghalei[3,4], Matthew C. Johnson[1,5], Katrin Karbstein[3,6,7] and M. Elizabeth Stroupe[1,7]

[1] Department of Biological Science and the Institute of Molecular Biophysics, Florida State University, Tallahassee, Florida, 32306

[2] these authors contributed equally

[3] Department of Integrative Structural and Computational Biology, The Scripps Research Institute, Jupiter, Florida, 33458

[4] Present address: Emory University School of Medicine, Department of Biochemistry, Atlanta, Georgia

[5] Present address: University of Washington, Department of Biochemistry, 1959 NE Pacific Street, Box 357350, Seattle, WA 98195

[6] HHMI Faculty Scholar

[7] To whom correspondence should be addressed: kkarbst@scripps.edu; mestroupe@bio.fsu.edu

RUNNING TITLE

Structure of an 80S-like ribosome assembly intermediate

ABSTRACT

During their maturation, nascent 40S subunits enter a translation-like quality control cycle, where they are joined by mature 60S subunits to form 80S-like ribosomes. While these assembly intermediates are essential for maturation and quality control, how they form, and how their structure promotes quality control remains unknown. To address these questions, we determined the structure of an 80S-like ribosome assembly intermediate to an overall resolution of 3.4 Å. The structure, validated by biochemical data herein, resolves a large body of previously paradoxical data and illustrates how assembly and translation factors cooperate to promote the formation of an interface that lacks many mature subunit contacts but is stabilized by the universally conserved Dim1. The structure also shows how this interface leads to unfolding of the platform, which allows for temporal regulation of the ATPase Fap7, thus linking 40S maturation to quality-control during ribosome assembly.

(Introduction)

Ribosome assembly is a highly regulated process, which begins with transcription, processing, and folding of the rRNA in the nucleolus. Coupled to these co-transcriptional events is the binding of most ribosomal proteins. These processes are facilitated, coordinated and regulated via a large machinery of nearly 200 assembly factors (AFs), which bind transiently to nascent ribosomes. After these co-transcriptional events are completed, largely assembled precursors retaining seven AFs are exported into the cytoplasm, where they undergo final maturation (1, 2). These final maturation steps are coupled to quality control steps in a translation-like cycle (3-5). In this cycle, nascent 40S ribosomes bind mature 60S subunits in an eIF5B-dependent manner to produce 80S-like ribosomes (3, 4), the substrates for rRNA maturation and quality control by the essential ATPase Fap7. By binding 80S-like ribosomes and inducing structural changes that release the AF Dim1, Fap7 tests the ability of newly-made ribosomes to adopt conformations critical to translocation of the mRNA through the ribosome. Bypass of this step allows for release of defective ribosomes into the translating pool (5).

Recently, structural information has proliferated on very early nucleolar (6-8), as well as initial cytoplasmic 40S assembly intermediates (9-13), however no structural information has been available for 80S-like ribosomes, despite their central role for quality control and maturation. Thus, it remains unclear how they are formed despite the presence of key component AFs that block subunit joining. Furthermore, how they enable the temporal regulation of Fap7 activity is also unknown.

Here, we use single-particle cryogenic electron microscopy (cryo-EM) to visualize the structure of 80S-like ribosomes that accumulate after depletion of the essential ATPase Fap7 (5). The structure is validated by biochemical data herein, as well as previous structural and biochemical data, and illuminates how 80S-like ribosomes harboring the key AFs Dim1 and Tsr1 form, despite their position that blocks joining in earlier assembly intermediates. Furthermore, structural and biochemical data also reveal how the formation of 80S-like ribosomes enables rRNA maturation and quality control.

RESULTS AND DISCUSSION

To better understand how 40S ribosomes are matured and how this maturation is quality-controlled via structural and functional mimicry of translation events, we used single-particle cryo-electron microscopy (cryo-EM) to visualize the structure of 80S-like ribosomes. These ribosome assembly intermediates were accumulated by depletion of the essential ATPase Fap7 (4, 5), and were purified via a TAP-tag on the AF Tsr1 (5). SDS-PAGE analysis coupled to mass-spectrometry and Western blotting demonstrates that these 80S-like ribosomes retain the AFs Tsr1, Dim1 and Pno1. Nob1 is highly substoichiometric (**Extended Data Figure S1a)**. Additionally, 60S ribosomal proteins and ribosome associated factors such as the SSA/SSB chaperones were identified, consistent with the previously demonstrated presence of 25S rRNA (5). Importantly, previous biochemical data have already confirmed that these assembly intermediates are on pathway, as addition of recombinant Fap7 and ATP to these 80S-like ribosomes leads to the release of Dim1 and the formation of a hybrid-like state (5).

Initial three-dimensional alignment and classification identified two populations of particles. One was refined to a resolution of 3.6 Å, had features similar to mature 80S ribosomes (**Extended Data Figure S1b-d**), and was similar to a recently noted 80S pre-ribosome lacking AFs (12). In this subclass of pre-ribosomes that lacked the AFs Tsr1, Dim1 and Pno1, the platform, beak, decoding helix, and bridge B3 are in their mature conformation and there is no density for a tRNA in any position (**Extended Data Figure S1e**). This subclass will not be discussed further.

The other subclass had strong 60S density but weaker pre-40S density. Further refinement of the small or large subunit alone by masking out the density of the other subunit improved the clarity of the small subunit to an overall resolution of 3.7 Å and the large subunit to an overall resolution of 3.4 Å (**Extended Data Figure S1f**). Although the particles showed no preferred orientation from cryogenic preservation, the resolution of the small subunit remained anisotropic, with local resolutions ranging from ~3.4 Å at its core to ~8.5 Å at the interface and the platform (**Extended Data Figure S1g-l)**. Therefore, we performed local classification at these regions as described in detail in the methods. The results of this local classification are described in the Figures below.

Movements of the small subunit relative to the large subunit

The improvement in resolution when the pre-40S subunit was refined in isolation indicated that it is mobile relative to the large subunit. Subsequent multi-body analysis (14) indicated several independent motions of pre-40S relative to 60S. Most of these can be described by the first three Eigen vectors that correspond to three independent motions (**Extended Data Figure S2a**). 40S is mobile relative to 60S in mature ribosomes (14); however, the motions that pre-40S undergoes in this intermediate are more extreme, because there are fewer subunit bridges formed in this assembly intermediate (see below), enabling a larger range of motion. Further, while the 40S head moves independently from the body in mature ribosomes (14), in 80S-like pre-ribosomes pre-40S moves as a rigid body, rotating both outward from 60S and parallel to the interface (**Extended Data Figure S2b**). This may be because by binding both the head and the body, Tsr1 holds them in a rigid position with respect to each other. Additionally, or alternatively, the neck, a key point of movement, has not yet formed (see below). The movement described by the first Eigen vector somewhat resembles that occurring during translocation, albeit more exaggerated. Importantly, the position of the pre-40S relative to the 60S subunit is consistent with our previous solution footprinting data, which showed that 80S-like ribosomes are in a classic-like state (5). In fact, in the composite position of pre-40S relative to 60S, 80S-ribosomes appear to be hyper-classic (positioned away from the rotated state by a 23^{o} counter-clockwise rotation from the classic state, **Extended Data Figure S3**).

80S-like pre-ribosomes are joined via an immature interface

Previous structural analyses had demonstrated that the AFs Dim1 and Tsr1 block 60S subunit joining: Dim1 by sterically blocking the 60S, Tsr1 by blocking eIF5B, as well as by stabilizing a conformation of h44 where it is "pulled out" of the subunit interface, thereby sterically clashing with 60S subunits as well as perturbing the many subunit bridges on h44 (10-13). To accommodate these AFs, and most notably h44 in 80S-like ribosomes, the pre-40S subunit is opened away from the 60S, creating space between the subunits and allowing for movement of Tsr1 and Dim1 relative to their position in isolated pre-40S ribosomes (**Figure 1a-c**). As a result, the subunit interface in 80S-like pre-ribosomes is formed by fewer intersubunit bridges than in mature 80S. Because the pre-40S subunit head is positioned far from the central protuberance of the mature 60S, the B1a, b, and c bridges, which involve the 40S head, are not yet formed (**Figure 1d**). Similarly, the pre-40S is turned away from the 60S on the platform side and moved towards it on the beak side. As

a consequence, bridge B7a cannot form because that side of the head is now too distant from the 60S (**Figure 1c-d)**. Further, the novel position of pre-40S relative to 60S accommodates the immature position of h44, which is shifted left, thus preventing formation of the bridges at the top of h44, including B3 and B5 (**Figure 1b-d**) (10, 12). In contrast, the eukaryote-specific bridges at the 40S foot are largely maintained, including eB8, eB10, eB11, eB12, and eB13 (**Figure c-d)**. In the case of a B5/B8-like bridge between h44 and Rpl23/uL14 and a B6-like bridge between h44 and Rpl24, the intersubunit connections are shifted due to the novel orientations of the two subunits but involve analogous interactions between the same structural elements (**Figure 1d and Extended Data Figure S4**).

The most surprising difference between this 80S-like assembly intermediate and the mature 80S ribosome is the change in the interaction of H69 from the large subunit with the small subunit. H69 is the target of RRF (15), which dissociates ribosomes as well as some antibiotics (16-18), demonstrating its central role for the stability of 80S ribosomes. In mature 80S ribosomes, H69 forms an A-minor interaction with h44 (19) to establish the B2a bridge. In contrast, in 80S-like pre-ribosomes, H69 binds h24 (**Figure 1e-f**), which is substantially moved from its mature position (see below).

Although the map at the subunit interface is of lower resolution than the rest of the molecule, thereby preventing us from precisely modeling atomic interactions between H69 and h24, the map nevertheless allows us to assign the densities to H69 and h24 with high confidence. H69 is positioned exactly as it is in mature ribosomes. The local resolution of this helix at about 5.5 Å, somewhat lower than the 60S as a whole but nonetheless high enough to confidently model the existing H69 into the density (**Figure 1f and Extended Data Figure S1k**). While the tip of h24 is at lower resolution (~7.5 Å), the map nonetheless demonstrates a link between the bottom of h24, which is well-resolved, and H69, strongly suggesting that the RNA that binds H69 is the top of h24 (**Figure 1f and Extended Data Figure S1k**). Of note, we have also validated interactions between Dim1 and h24 as well as Dim1 and the 60S subunit in biochemical experiments described below.

Dim1 stabilizes the repositioning of h24 and binds the 60S subunit

Dim1's position in pre-40S subunits inhibits subunit joining by sterically blocking the approach of H69 from the 60S subunit (10-13). As described above, the position of H69 is unchanged, and it remains the main connection between the subunits in 80S-like ribosomes. Thus, if Dim1 remained at the same position it would still block subunit joining, despite the remodeled interface. To clarify the position of Dim1 in 80S-like ribosomes, we performed extensive localized classification and refinement as described in the methods. Although the resolution remains relatively low (~8.5 Å), this analysis shows that Dim1 moves with h24 (**Figure 2a-c, Supplemental Movie 1**). The rotation of h24 away from the platform repositions Dim1 above H69, alleviating the steric conflict. In addition, this movement essentially releases Dim1 from the pre-40S subunit, maintaining contact only with h24 and instead, promoting its interaction with the large subunit.

To validate the position of Dim1 in this relatively low-resolution portion of the map and probe the importance of the newly established contacts between Dim1 and h24, as well as Dim1 and the 60S subunit for formation of 80S-like ribosomes, we created variants in Dim1 and tested their effects on yeast growth and subunit joining. The residues mutated in Dim1-FRK (F231L, R233E, K234E, orange in **Figure 2d-e**) are oriented towards h24 in 80S-like ribosomes, but do not form interactions in pre-40S ribosomes. The residues mutated in Dim1-IKN (I250A, K253A, N254A, yellow in **Figure 2d-e**) are oriented across the interface toward Rpl11 and the extreme C-terminus of Rpl42 in the 60S subunit, highlighting the role Dim1 plays in stabilizing this intermediate. Again, these residues do not form major interactions in pre-40S ribosomes. These variants were tested using a yeast strain where both Fap7 and Dim1 are galactose-inducible, glucose-repressible. This strain was supplemented with plasmids encoding for wild type or mutant Dim1, and either no Fap7 or inactive Fap7. To test if the mutated residues are important for subunit joining, we co-depleted endogenous Fap7 and endogenous Dim1, such that plasmid-encoded Dim1 was the only Dim1 source. In otherwise wild type yeast, depletion (or inactivation) of Fap7 leads to the accumulation of pre-40S ribosomes in 80S-like complexes, as indicated by the co-sedimentation of pre-18S rRNA and 25S rRNA in 80S-sized fractions (4). This accumulation of 80S-like ribosomes is dependent on the ability to form 80S-like ribosomes (4, 5). Both the Dim1-FRK and the Dim1-IKN variants strongly impair the formation of 80S-like ribosomes (**Figure 2f-g)**. Thus,

these biochemical data validate the position of Dim1 and its interactions with h24 and the 60S subunit.

Tsr1 promotes the formation of the opened interface

In earlier 40S assembly intermediates, the AF Tsr1 binds parallel to h44, between the 40S body and beak, and interacts with another AF, Rio2 (10-13) (**Figure 3a-b and Extended Data Figure S5a**). The core density for Tsr1 is strong (**Figure 3b**), allowing us to position Tsr1 with confidence. In these earlier structures, Tsr1's N-terminal □-helix is inserted behind h44, forcing h44 away from the body, thereby blocking the formation of canonical 80S ribosomes (11, 13, 20). In 80S-like pre-ribosomes, which have released Rio2, Tsr1 is no longer attached to the beak. Instead it is repositioned towards the tip of the beak via a rigid-body movement around a hinge at Ala63 within the N-terminal helix, which remains under h44 (**Figure 3a, Extended Data Figure S5b, and Supplemental Movie 2**).

To test the importance of this hinge rotation for formation of 80S-like ribosomes, we deleted the Tsr1 N-terminal helix (Tsr1-ΔN74) and tested the effect on cell growth and formation of 80S-like ribosomes using yeast strains where endogenous Tsr1 is under a galactose-inducible, glucose-repressible promoter and wild type or mutant Tsr1 is provided on a plasmid. The data in **Figure 3c** show that deletion of the N-terminal helix produces a lethal growth phenotype. To test whether deletion of the hinge-helix affected subunit joining, we used sucrose gradient fractionation as described above in yeast strains where Fap7 could be co-depleted. In wild type yeast that are competent for subunit joining, depletion of Fap7 will lead to the formation of 80S-like ribosomes, except in strains where the formation of 80S-like ribosomes is blocked, such as the eIF5B deletion strain (4). This assay demonstrates that subunit joining is blocked in Tsr1-ΔN74 (**Figure 3d).** Thus, rotation around the hinge in Tsr1 is essential for the formation of 80S-like ribosomes.

Interestingly, our previous dataset of earlier 40S assembly intermediates (11) contains a small population of molecules in which Tsr1 appears to be similarly rotated (**Extended Data Figure S6a**). In this low-resolution structure Tsr1 has a disordered C-terminal domain either due to its mobility in isolated pre-40S and/or owing to the small number of particles that contribute to the

structure. Nonetheless, this observation suggests that Tsr1's movement away from h44 and the beak is intrinsic to Tsr1 and not induced by eIF5B, but perhaps stabilized by it.

The positioning of Tsr1 in the previously described earlier 40S assembly intermediates is incompatible with eIF5B binding (20). Nonetheless, eIF5B is required for the formation of 80S-like ribosomes (3, 4). To better understand if the repositioning of Tsr1 to the beak enables the binding of eIF5B, we docked eIF5B into this 80S-like pre-ribosome structure by superimposing the 60S subunits in our complex and the previously visualized mature 80S•eIF5B complex (21). (Note that the present intermediate accumulates after eIF5B has dissociated in a GTPase-dependent manner.) This analysis suggests that the postulated clashes between Tsr1 and eIF5B (20) are largely resolved in these 80S-like ribosomes. Surprisingly however, it is not the repositioning of Tsr1 towards the beak that provides this steric relief. Instead, it is the opened subunit interface that allows for the concurrent binding of Tsr1 and eIF5B (**Figure 3e-f),** by providing space for eIF5B behind Tsr1 at the subunit interface.

In summary, the structure of 80S-like ribosomes clarifies multiple roles for Tsr1 in the formation of 80S-like ribosomes (versus canonical 80S ribosomes): first, Tsr1 forces out h44, thereby sterically preventing the subunits from approaching each other more closely to form the canonical subunit bridges in the head (**Figures 1a, 3a-b, and Extended Data S5**); second, Tsr1 stabilizes the interface due to its interaction with both pre-40S and 60S (**Extended Data Figure S6b)**; third, Tsr1 blocks access of eIF5B to its typical binding site on 40S, instead enforcing a position of eIF5B that blocks the formation of the B3 bridge (**Figure 3e-f**). The B3 bridge is a strong and early-forming bridge (22), therefore Tsr1 steers the subunits into 80S-like ribosomes by promoting a different position of eIF5B. Together, the structure suggests that while Dim1 stabilizes 80S-like ribosomes, Tsr1 functions to induce the formation of these complexes.

rRNA folding and protein assembly to the nascent 40S subunit

Previous structures showed that earlier pre-40S subunits lack Rps10 (eS10), Rps26 (eS26) and Asc1 (4, 10-13) and that the tip of h31 remains unfolded (10, 12). In this intermediate, clear density for Asc1 and Rps10 is apparent at their mature position in the head (**Extended Data Figure S7**), indicating that these proteins are recruited prior to Fap7 activity, as expected based on our previous

biochemical analyses (4). Furthermore, the tip of h31 is clearly visible (**Extended Data Figure S8**). This coincides with the beak moving forward to its mature position while the overall head configuration straightens (**Extended Data Figure S9**), movements that occur where the 40S head joins the body near the Tsr1 and Rio2 binding sites. Specifically, in earlier pre-40S intermediates Tsr1 binds immediately adjacent to the last ordered nucleotide in h31 and Rio2 is bound adjacent to where the helix is located in mature 40S subunits (10-13). We suggest that these changes arise from dissociation of Rio2 and detachment of Tsr1 from the head in 80S-like pre-ribosomes, indicating roles for these two maturation events in promoting the folding of h31.

The platform is substantially unfolded

Extensive differences between earlier pre-40S subunits and the 80S-like ribosomes analyzed here are also observed at the platform, where a rigid body motion opens the platform towards the large subunit (**Figure 4a-c**). This movement is presumably facilitated by the repositioning of h24 from the platform to the subunit interface (see above), and accompanied by disorder in the tip of h23, and partial loss of Rps1 and Rps14, as previously observed (4), requiring local classification to improve its resolution. The other major subclass of 80S ribosomes we observe in our preparations has a canonical platform (**Figure S1e**), ruling out artifacts during sample purification or preparation for cryo-EM as causative for the platform rearrangements described below. Furthermore, no preferential orientation in the molecules were observed, as expected if a subpopulation of molecules were interacting preferentially with the air-water interface thus unfolding the platform (**Extended Data Figure S1g**). We therefore conclude that these changes represent folding transitions during 40S subunit maturation.

To interpret the density at the platform, we used rigid body fitting to place the Rps1•Rps14 •Pno1 complex from the earlier pre-40S intermediates in the platform density, essentially assuming that interactions between Rps14 and Pno1 remain unaltered in 80S-like ribosomes. To validate this assumption, we produced mutants in the Rps14•Pno1 interface (**Figure 4d**). These include Rps14-R107E as well as Pno1-QDF (Q153E, D157R, F237A). These variants were tested for their effects on cellular growth in galactose-inducible, glucose repressible Rps14 and Pno1 strains, respectively. These experiments demonstrate severe growth phenotypes for these mutants (**Figure 4d**). Because both Rps14 and Pno1 are bound (but do not yet interact) in early 90S precursors (6-

8), we used Northern analysis to confirm that the effects from these mutations do not arise from early maturation events. Rps14 and Pno1 depletion both have very early assembly defects, which preclude the formation of 20S rRNA ((23-25), **Extended Data Figure S10**). This analysis demonstrates that both mutants produce 20S rRNA to nearly wild type levels (**Extended Data Figure S10**). Thus, the lethal or near-lethal growth defects from these mutants do not arise from early maturation defects. Next, we used sucrose-gradient fractionation to ask if Pno1 is bound more weakly to 80S-like ribosomes in these mutants. 80S-like ribosomes were accumulated via depletion of Fap7 as previously described (4), and Western analysis was used to probe the sedimentation of Pno1 with pre-ribosomes (40S and 80S-like fraction), or dissociated Pno1. As expected from a weakened Pno1•Rps14 interface, the fraction of free Pno1 is increased in both the Pno1-QDF and Rps14-R107E mutant (**Figure 4e-f**). These data strongly suggest that the Pno1•Rps14 interface is maintained in 80S-like ribosomes, supporting the placement of the Rps1•Rps14•Pno1 complex in the platform density (**Figure 4c).**

Further analysis of this opened platform structure illuminates the function of the ATPase Fap7 in the release of Dim1 (5). We have previously shown that Fap7 bridges Dim1 and Rps14, presumably reflecting the recruitment of Fap7 by Rps14 to promote Dim1 release (5). Thus, we asked if on these 80S-like ribosomes Fap7 could be positioned between Dim1 and Rps14. By docking the previously solved crystal structure of the Fap7•Rps14 complex (26) onto Rps14, Fap7 is positioned adjacent to Dim1 (**Figure 5a**), as predicted by our biochemical data (5). Intriguingly, only one of the two observed interfaces in the Fap7•Rps14 structure (there are 4 complexes in the asymmetric unit) allows for docking of Fap7 onto 80S-like ribosomes, while the other interface produces a steric clash (**Figure 5a and Extended Data Figure S11a**).

To validate the docked structure of Fap7, we created point mutations in Fap7 and Rps14 that would affect this interface (**Figure 5b**). Rps14-K49E and Fap7-RYD (R114E, Y116A, D118K) alter amino acids that contact their binding partners only in the dockable interface, while Rps14-RVM (R41E, V42L, M46A) alters an arginine that binds Fap7 in both interfaces (Val42 and Met46 only bind Fap7 at the dockable interface) (**Figure 5b and S11b**). Each mutation provides a substantial growth phenotype (**Figure 5c**). Furthermore, recombinant Fap7-RYD and Rps14-RVM block binding of Rps14 and Fap7, respectively (**Figure 5d**). Finally, as observed for inactive Fap7 (5),

the growth phenotype from Fap7-RYD is partially rescued by a self-releasing mutation in Dim1, Dim1-EKR (**Figure 5e**). Together, these experiments validate the docking of Fap7(•Rps14) onto Rps14 in 80S-like ribosomes (**Figure 5a**). In addition, because this independently and biochemically validated the position of Fap7 binds both Rps14 and Dim1, thereby reproducing the previously observed biochemical interactions between these three proteins (5), it also validates the interpretation of the medium-resolution features of the map: Rps14 on the platform and Dim1 at the subunit interface.

Fap7 binds Rps14 (5, 26, 27), and the biochemical data above demonstrate the importance of this interaction for its function in 40S maturation and Dim1 release. Rps14 is found in essentially its mature position in the earliest 40S assembly intermediates (6-8), thus raising the question how the specific recruitment of Fap7 to 80S-like ribosomes is achieved. Docking Fap7 onto earlier pre-40S intermediates demonstrates that it would clash with the platform, in particular the tip of h23 (**Extended Data Figure S11c**). Comparison to the interaction of Fap7 with Rps14 in 80S-like ribosomes indicates that this steric conflict is relieved by opening of the platform, which repositions Rps14, and mobilizes h23. Thus, the unfolding of the platform in 80S-like ribosomes allows for the temporal regulation of Fap7 binding and activity to 80S-like ribosomes (**Figure 5f**).

In summary, the structure of 80S-like pre-ribosomes presented here, validated by genetic and biochemical data herein, as well as previous biochemical (5), mass spectrometry (4) and crystallographic (26) data, reveal multiple unexpected features that allow for the reconciliation and explanation of multiple previous observations. (i) 80S-like ribosomes display an opened interface whose formation is enabled by the AF Tsr1. Tsr1 blocks the canonical binding mode of eIF5B, required for subunit joining, supports a structure of the decoding helix that requires an opened interface, and stabilizes the complex by binding both subunits extensively. (ii) The most unexpected feature of the subunit interface in 80S-like ribosomes is the novel interaction of H69 from the large subunit with h24 from the small subunit, which is stabilized by the AF Dim1; because h24 is a component of the platform region, this interaction opens the platform towards the large subunit and mobilizes constituent RNA and protein structures. (iii) The remodeling of the platform allows for temporal regulation of the binding of the ATPase Fap7, which functions in quality control of nascent 40S subunits by linking the dissociation of Dim1 to the ability to carry

out conformational changes associated with translation (5). Thus, this structure finally explains how the formation of 80S-like ribosomes is required proofreading of 40S ribosome maturation.

MATERIALS AND METHODS

Yeast strains and cloning: The yeast strains (Gal::Fap7;Gal::Dim1, Gal::Fap7;Tsr1TAP, Gal::Fap7, Gal::Tsr1, Gal::Pno1, ΔRps14B;Gal::Rps14A, Gal::Fap7;Gal::Pno1, and ΔRps14B;Gal::Rps14A;Gal::Fap7) were produced using PCR-based recombination (28), and confirmed by PCR and western blotting. Mutations in Dim1, Fap7, Tsr1 Pno1, and Rps14-containing plasmids were introduced by site-directed mutagenesis and confirmed by sequencing.

Quantitative growth assays: Doubling times of cells were measured essentially as described before (5). Cells were first grown to mid-log phase in glucose drop-out media and then inoculated into YPD. Growth was measured in a Synergy 2 multi-mode microplate reader (BioTek). Doubling times and statistical analysis were performed using GraphPad Prism version 6.02, GaphPad Software, La Jolla, California USA, www.graphpad.com.

Sucrose density gradient analysis: Sucrose gradient fractionations of whole cell lysates, followed by Northern blot analysis, were performed as described previously (4). To calculate the amount of 20S rRNA in the 80S-like fraction, the signal in the 40S fraction (fractions 3-4) and the 80S fraction (fractions 6-7) were quantified using Quantity One 1-D Analysis Software version 4.1.2 (Basic) from Bio-Rad Laboratories, Inc.. The 80S signal was then divided by the sum of the 80S and 40S signal.

Antibodies: Antibodies against soluble recombinant Dim1, Nob1, Pno1, Rio2, and Tsr1 were raised in rabbits by Josman LLP, and HRP-conjugated anti-rabbit and anti-mouse secondary antibody was obtained from Rockland Immunochemicals. Antibody against Rpl3 was a gift from J. Warner. Antibody against eEF2 was a gift from T. Goss-Kinzy.

Protein expression and purification: MBP-Fap7 and MBP-Fap7-RYD were expressed and purified as previously described (5). SUMO-Rps14 was expressed in Rosetta DE3 cells, induced by addition of 1mM IPTG and grown for 5 hours at 30˚C. For purification, cells were lysed by sonication in Ni^{2+}-NTA lysis buffer supplemented with 0.5 mM phenylmethylsulfonyl fluoride (PMSF) and 1 mM benzamidine. The cleared lysate was purified over Ni^{2+}-NTA resin (QIAGEN) and eluted in lysis buffer supplemented with 200 mM imidazole. The eluted protein was dialyzed into 50 mM Tris pH 8.0 and 150 mM NaCl and then purified using a Mono S column equilibrated in dialysis buffer. The protein was eluted with a linear gradient from 150 mM to 1 M NaCl and then further purified by gel filtration on a Superdex 75 column equilibrated in 50 mM Tris pH 8.0, 200 mM NaCl, 2 mM DTT, and 1 mM TCEP. The protein was stored in gel filtration buffer supplemented with 15% glycerol. SUMO-Rps14-RVM was purified using the same protocol as the wild-type protein.

Protein binding assays: Protein binding assays were performed as previously described (5). In brief, 3 μM MBP-Fap7 or MBP-Fap7-RYD were mixed with 4.4 μM SUMO-Rps14 or SUMO-

Rps14-RVM in binding buffer (50 mM Tris, pH 7.5, 150 mM NaCl, and 5% glycerol) and applied to amylose resin. Resin was washed with binding buffer and bound proteins were eluted in binding buffer supplemented with 50 mM maltose.

Cryo-EM sample purification and preparation: Fap7 was depleted by growth in YPD for 16 hours. 2.5 mL of lysis buffer (30 mM HEPES-KOH pH 6.8, 100 mM NaCl, 6 mM $MgCl_2$, RNasin, PMSF, Benzamidine, EDTA – free protease inhibitor tablet (Santa Cruz Biotechnology, Dallas, TX, USA), Leupeptin, Pepstatin, and Aprotinin was added to 4 g of lysed frozen cell powder. The cell powder was mixed with 2 mL of Zircona silica beads (Millipore-Sigma, St. Louis, MO, USA) and vortexed 20 sec for homogenization. The frozen cell lysate thawed at 4 ˚C on a rocker. Thawed cell lysate was cleared via two centrifugations at 4˚C: first, at 3,000 x g for five min and second, at 10,000 x g for 10 min. The cleared supernatant was incubated with 250 µL of pre-equilibrated IgG beads (GE Healthcare, Little Chalfonte, UK) at 4˚C for 1.5 h with gentle rotation. After incubation, the flow through was discarded and beads were washed three times with buffer A (30 mM HEPES-KOH pH 6.8, 100 mM NaCl, 6 mM $MgCl_2$, 0.075% NP-40, PMSF, Benzamidine) followed by an additional wash buffer B (30 mM HEPES-KOH pH 6.8, 100 mM NaCl, 6 mM $MgCl_2$, PMSF, Benzamidine). Washed beads were incubated with 250 µL TEV cleavage buffer (30 mM HEPES-KOH pH 6.8, 100 mM NaCl, 6 mM $MgCl_2$, PMSF, Benzamidine, 1 mM DTT and 0.5 mM EDTA) supplemented with 2.5 µL AcTEV protease (Invitrogen, Carlsbad, CA, USA) at 16˚C for two hours with gentle shaking. After incubation, flow through was collected. The concentration and quality of eluate was determined spectrophotometrically using a Nanodrop 1000 (Thermo Scientific, Waltham, MA, USA). 3 µL of eluate (72 nM) was applied to a plasma-treated UltraAuFoil 1.2/1.3 grid (Quantifoil, Großlöbichau, Germany). The grids were hand blotted for 3 sec from the backside of the grid before being plunged into liquefied ethane.

Microscopy and image pre-processing: Images were acquired on an FEI Titan Krios transmission electron microscope operated at 300 kV equipped with a DE64 (Direct Electron, San Diego, CA, USA) directed by the automated hole finder in Leginon (**Extended Data Tables 1-4**) (29). Images were recorded in "movie mode" at a range of -1.3 to -2.5 µm defocus. A total of 25 $e^-/Å^2$ dose was spread over 42 frames at a nominal magnification of 59,000x, yielding a pixel size of 1.24 Å/pixel at the specimen level. The images that showed signs of astigmatism, poor ice, drift, empty holes or bad sample quality were discarded. In total, 4,193 micrographs were selected for frame alignment and dose compensation with the MotionCorr algorithm (30). Initial CTF parameters were estimated using Gctf (31). A total of 146,641 particles were selected by the auto-picking algorithm implemented and further processed in Relion-3.0, with per-particle CTF estimation and correction and beam-tilt correction (32). 3D classification and 3D autorefine revealed 55,949 particles whose 60S and 40S subunits were at an orientation like mature 80S (empty pre-ribosomes) (**Figure 1c and Extended Data Figure 1b, d**), as was seen before (12). 90,692 particles had strong 60S density but diffuse 40S density (80S-like ribosomes) (**Figure 1c and Extended Data Figure 1b, d**).

Refinement of the parent structure and individual subunits: Both empty pre-ribosomes and 80S-like ribosomes were independently subjected to refinement using Relion-3's "autorefine" function. The empty pre-ribosome structure was refined to 3.6 Å resolution (**Extended Data Figure 1b, f, i, and j**). The 80S-like pre-ribosome structure (parent structure) was refined to 3.4 Å resolution, but with significant anisotropy in the pre-40S subunit (**Extended Data Figure 1b, f, i, and j**). To

better resolve the individual subunits, the 80S-like pre-ribosome structure was further refined either with a 3D custom mask on the 40S subunit or with a mask on the 60S subunit, yielding a structure of pre-40S at 3.7 Å-resolution and a structure of 60S at 3.4 Å resolution (**Extended Data Figure 1b, f, i, and j**). To further analyze the nature of the anisotropy in the 80S-like ribosome, the parent structure was further refined with the multi-body approach implemented in Relion-3 using two masks. A mask on 60S that included the bridge density was used as the first body and a 3D mask on pre-40S as second body with an 11 Å overlap (**Extended Data Figure S2**).

Local classification and refinement: To better define the central density that bridges the two subunits, we binned the image stack by factor 2 and performed further 3D classifications without alignment using a spherical mask that included H69 from 60S and the space where the now unfolded h45 is located in pre-40S. A single, dominant subclass (43,893 particles) emerged that, after further autorefinement using a custom 3D mask on 60S subunit including H69 in Relion3.0 (**Extended Data Figure S1b**), revealed the position of Dim1 at the central bridging density still bound to the repositioned h24 (**Extended Data Figure S1k**). Although the resolution of Dim1 remains relatively low (~8.5 Å), the density has the size, and shape of Dim1 (**Figure 2b and Extended Data Figure S1k)**, and Western-blot analysis (**Extended Data Figure S1a)** demonstrates the presence of Dim1 in the complex. Furthermore, as described in detail in the results, the interactions between Dim1 and h24 are largely preserved in this structure and the previous pre-40S structures. H69 also has a resolution of ~5.5 Å and the contours of the major and minor grooves of the hairpin are clearly visible without any localized classification. Finally, the repositioned h24 has a resolution of ~8.5 Å and the twist of the helix is also visible without any localized classification. Despite being at lower resolution than the core structure, these key central elements are clearly identifiable within the limits of the resolution because of the clear connectivity to well-resolved parts of the structure, the distinct helical contours of the RNA helices and the two-domain construction of Dim1.

Similarly, to improve the density on the pre-40S platform, we performed 3D classification without alignment using a spherical mask including only the platform. A single, dominant class (36,914 particles) showed the better-defined platform region after further autorefinement using a custom 3D mask on pre-40S (**Extended Data Figure S1b and l**). Again, although at lower resolution than the core of the molecule (**Extended Data Figure 1l**), the density follows the contours of an unchanged Rps1•Rps14•Pno1 complex repositioned as a rigid body. Mutagenesis supports our assumption that the complex remains intact (**Figure 4c-f and Extended Data Figure 10**).

Model building

Pre-40S and 60S were independently modeled from the rotated, mature 80S ribosome (PDB ID 3J77 (21, 33) First, subunits were rigid-body rotated into either half of the map to assess their relative orientation at the newly formed interface. 60S fit well with a few minor adjustments to Rpl19, H69, and the L1 stalk. For Rpl19, the alpha helical tail was manually fit into the newly-formed bridge in Coot (34). The L1 stalk was rotated as a rigid body to fit the density. Then, the density was segmented from the main map with the "segmentation" tool in Chimera (35). The coordinates for the L1 stalk were isolated from the remainder of the model and then rigid body fit into the density with the "fit in map" tool in Chimera, then re-joined to the main model manually. H69 was manually rotated in Coot to match the curve of the bridge density. The chain for Rlp41 was manually removed.

Pre-40S also required some adjustments to h24, the head, and Tsr1. No density was apparent for h23, Rps1, Rps26, or Rps14 in the consensus map so they were removed from the model. In Coot, h24 was rotated as a rigid body with minimal changes to match the contours of the remodeled bridge. The head density was segmented from the body from the main map with the "segmentation" tool in Chimera. The coordinates for the head rRNA and r-proteins were isolated from the remainder of the model and then rigid body fit into the density with the "fit in map" tool in Chimera, then re-joined to the main model manually. Tsr1 from the pre-40S ribosome (PDB ID 6FAI (12)) was rigid-body fit into the density joining the head to the body. Human Dim1 from PDB ID 6G18 (9) was used to model a yeast Dim1 in SwissModel because there is no atomic resolution structure of yeast Dim1. After rigid-body fitting into the bi-lobed density at the main subunit bridge, the secondary structure elements (a-helices and b-sheets) were manually placed using Coot (34) into the density, followed by refinement with the Phenix.real.space.refine algorithm (36). The resulting model matched the density with a correlation coefficient (CC) of 0.8. The Rps1Rps14Pno1 trimer was rigid-body-fit into the segmented platform density using the "fit-in-map" feature in Chimera (35). The resulting model matched the density with a CC of 0.6. Each 60S or pre-40S model was then independently subjected to real space refinement against the best 60S or pre-40S map using the Phenix.real.space.refine algorithm (36). The resulting pre-40S model had 89.7% amino acids in favored Ramachandran Plot regions and 0.2% in the outlier region. The overall Clashscore was 13.0%. The resulting 60S model had 85.9% amino acids in favored Ramachandran Plot regions and 0.2% in the outlier region. The overall Clashscore was 27.9%.

All structure figures were made in Chimera (35) and assembled in Photoshop (Adobe, San Jose, CA) without additional modification.

REFERENCES

1. Bassler J, Hurt E. Eurokaryotic Ribosome Assembly. Annu Rev Biochem. 2018.
2. Klinge S, Woolford JL, Jr. Ribosome assembly coming into focus. Nat Rev Mol Cell Biol. 2018.
3. Lebaron S, Schneider C, van Nues RW, Swiatkowska A, Walsh D, Bottcher B, et al. Proofreading of pre-40S ribosome maturation by a translation initiation factor and 60S subunits. Nat Struct Mol Biol. 2012;19(8):744-53.
4. Strunk BS, Novak, M. N., Young, C. L. and Karbstein, K. A Translation-Like Cycle is a Quality Control Checkpoint for Maturing 40S Ribosome Subunits. Cell. 2012;150(1):111-21.
5. Ghalei H, Trepreau J, Collins JC, Bhaskaran H, Strunk BS, Karbstein K. The ATPase Fap7 Tests the Ability to Carry Out Translocation-like Conformational Changes and Releases Dim1 during 40S Ribosome Maturation. Molecular cell. 2017;67(6):990-1000 e3.
6. Barandun J, Chaker-Margot M, Hunziker M, Molloy KR, Chait BT, Klinge S. The complete structure of the small-subunit processome. Nat Struct Mol Biol. 2017;24(11):944-53.
7. Cheng J, Kellner N, Berninghausen O, Hurt E, Beckmann R. 3.2-A-resolution structure of the 90S preribosome before A1 pre-rRNA cleavage. Nat Struct Mol Biol. 2017;24(11):954-64.
8. Sun Q, Zhu X, Qi J, An W, Lan P, Tan D, et al. Molecular architecture of the 90S small subunit pre-ribosome. Elife. 2017;6.
9. Ameismeier M, Cheng J, Berninghausen O, Beckmann R. Visualizing late states of human 40S ribosomal subunit maturation. Nature. 2018;558(7709):249-53.

10. Heuer A, Thomson E, Schmidt C, Berninghausen O, Becker T, Hurt E, et al. Cryo-EM structure of a late pre-40S ribosomal subunit from Saccharomyces cerevisiae. Elife. 2017;6.
11. Johnson MC, Ghalei H, Doxtader KA, Karbstein K, Stroupe ME. Structural Heterogeneity in Pre-40S Ribosomes. Structure. 2017;25(2):329-40.
12. Scaiola A, Pena C, Weisser M, Bohringer D, Leibundgut M, Klingauf-Nerurkar P, et al. Structure of a eukaryotic cytoplasmic pre-40S ribosomal subunit. Embo J. 2018;37(7).
13. Strunk BS, Loucks CR, Su M, Vashisth H, Cheng S, Schilling J, et al. Ribosome assembly factors prevent premature translation initiation by 40S assembly intermediates. Science. 2011;333(6048):1449-53.
14. Nakane T, Kimanius D, Lindahl E, Scheres SH. Characterisation of molecular motions in cryo-EM single-particle data by multi-body refinement in RELION. Elife. 2018;7.
15. Pai RD, Zhang W, Schuwirth BS, Hirokawa G, Kaji H, Kaji A, et al. Structural Insights into ribosome recycling factor interactions with the 70S ribosome. Journal of molecular biology. 2008;376(5):1334-47.
16. Borovinskaya MA, Pai RD, Zhang W, Schuwirth BS, Holton JM, Hirokawa G, et al. Structural basis for aminoglycoside inhibition of bacterial ribosome recycling. Nat Struct Mol Biol. 2007;14(8):727-32.
17. Prokhorova I, Altman RB, Djumagulov M, Shrestha JP, Urzhumtsev A, Ferguson A, et al. Aminoglycoside interactions and impacts on the eukaryotic ribosome. Proc Natl Acad Sci U S A. 2017;114(51):E10899-E908.
18. Wang L, Pulk A, Wasserman MR, Feldman MB, Altman RB, Cate JH, et al. Allosteric control of the ribosome by small-molecule antibiotics. Nat Struct Mol Biol. 2012;19(9):957-63.
19. Ben-Shem A, Garreau de Loubresse N, Melnikov S, Jenner L, Yusupova G, Yusupov M. The structure of the eukaryotic ribosome at 3.0 A resolution. Science. 2011;334(6062):1524-9.
20. McCaughan UM, Jayachandran U, Shchepachev V, Chen ZA, Rappsilber J, Tollervey D, et al. Pre-40S ribosome biogenesis factor Tsr1 is an inactive structural mimic of translational GTPases. Nature communications. 2016;7:11789.
21. Fernandez IS, Bai XC, Hussain T, Kelley AC, Lorsch JR, Ramakrishnan V, et al. Molecular architecture of a eukaryotic translational initiation complex. Science. 2013;342(6160):1240585.
22. Shaikh TR, Yassin AS, Lu Z, Barnard D, Meng X, Lu TM, et al. Initial bridges between two ribosomal subunits are formed within 9.4 milliseconds, as studied by time-resolved cryo-EM. Proc Natl Acad Sci U S A. 2014;111(27):9822-7.
23. Vanrobays E, Gelugne JP, Caizergues-Ferrer M, Lafontaine DL. Dim2p, a KH-domain protein required for small ribosomal subunit synthesis. Rna. 2004;10(4):645-56.
24. Woolls HA, Lamanna AC, Karbstein K. The Roles of Dim2 in Ribosome Assembly. J Biol Chem. 2011;286: 2578-86.
25. Antunez de Mayolo P, Woolford JL, Jr. Interactions of yeast ribosomal protein rpS14 with RNA. J Mol Biol. 2003;333(4):697-709.
26. Loc'h J, Blaud M, Rety S, Lebaron S, Deschamps P, Bareille J, et al. RNA mimicry by the fap7 adenylate kinase in ribosome biogenesis. PLoS Biol. 2014;12(5):e1001860.
27. Hellmich UA, Weis BL, Lioutikov A, Wurm JP, Kaiser M, Christ NA, et al. Essential ribosome assembly factor Fap7 regulates a hierarchy of RNA-protein interactions during small ribosomal subunit biogenesis. Proc Natl Acad Sci U S A. 2013;110(38):15253-8.
28. Longtine MS, McKenzie A, 3rd, Demarini DJ, Shah NG, Wach A, Brachat A, et al. Additional modules for versatile and economical PCR-based gene deletion and modification in Saccharomyces cerevisiae. Yeast. 1998;14(10):953-61.

29. Carragher B, Kisseberth N, Kriegman D, Milligan RA, Potter CS, Pulokas J, et al. Leginon: an automated system for acquisition of images from vitreous ice specimens. J Struct Biol. 2000;132(1):33-45.
30. Li X, Mooney P, Zheng S, Booth CR, Braunfeld MB, Gubbens S, et al. Electron counting and beam-induced motion correction enable near-atomic-resolution single-particle cryo-EM. Nature methods. 2013;10(6):584-90.
31. Zhang K. Gctf: Real-time CTF determination and correction. J Struct Biol. 2016;193(1):1-12.
32. Zivanov J, Nakane T, Forsberg BO, Kimanius D, Hagen WJ, Lindahl E, et al. New tools for automated high-resolution cryo-EM structure determination in RELION-3. Elife. 2018;7.
33. Svidritskiy E, Brilot AF, Koh CS, Grigorieff N, Korostelev AA. Structures of yeast 80S ribosome-tRNA complexes in the rotated and nonrotated conformations. Structure. 2014;22(8):1210-8.
34. Emsley P, Lohkamp B, Scott WG, Cowtan K. Features and development of Coot. Acta Crystallogr D Biol Crystallogr. 2010;66(Pt 4):486-501.
35. Pettersen EF, Goddard TD, Huang CC, Couch GS, Greenblatt DM, Meng EC, et al. UCSF Chimera--a visualization system for exploratory research and analysis. J Comput Chem. 2004;25(13):1605-12.
36. Adams PD, Afonine PV, Bunkoczi G, Chen VB, Davis IW, Echols N, et al. PHENIX: a comprehensive Python-based system for macromolecular structure solution. Acta Crystallogr D Biol Crystallogr. 2010;66(Pt 2):213-21.
37. Ghalei H, Schaub FX, Doherty JR, Noguchi Y, Roush WR, Cleveland JL, et al. Hrr25/CK1δ-directed release of Ltv1 from pre-40S ribosomes is necessary for ribosome assembly and cell growth. Journal of Cell Biology. 2015;208(6):745-59.

ACKNOWLEDGEMENTS

This work was supported by NIH grants R01-GM117093 and R01-GM086451, and HHMI Faculty Scholar grant 55108536 to K.K.. The authors acknowledge the use of instruments at the Biological Science Imaging Resource supported by Florida State University and NIH grants S10 RR025080, S10 OD018142, and U24 GM116788. H.G. was supported in part by a PGA National Women's Cancer Awareness Postdoctoral Fellowship. We wish to thank members of the Karbstein lab for comments on the manuscript, and Drs. Scott Stagg and Kenneth Taylor for useful discussions. J.R. and H.G. prepared samples; J.R. and M.E.S. carried out structure reconstruction; M.D.P., H.H. and S.C. carried out yeast analyses; M.C.J. performed cryo-EM analysis of pre-40S; K.K. and M.E.S. conceived of the experiments and wrote the paper.

COMPETING INTERESTS

The authors have no competing interests.

MATERIALS AND CORRESPONDENCE

Correspondence requests should be addressed to: M.E. Stroupe, mestroupe@bio.fsu.edu
Materials requests should be addressed to: K. Karbstein, kkarbst@scripps.edu

FIGURES AND LEGENDS

Figure 1: 80S-like ribosomes join via an immature interface. a. Overall structure of 80S-like ribosomes. 60S is light blue, pre-40S is yellow, Dim1 is dark blue, and Tsr1 is green. **b.** The pre-40S interface has only Tsr1 (green) and Dim1 (blue) bound. **c.** In 80S-like pre-ribosomes the space between the subunits is expanded. **d.** The bridges between 60S and the pre-40S head and central region of the body are largely not formed (blue patches) while those with the pre-40S foot remain intact or modestly reorganized (pink). **e.** In mature ribosomes, helix 69 from the 60S subunit (H69, blue) binds helix 44 from the pre-40S subunit (h44, yellow, model from PDB ID 3J77 (33)). 80S-like ribosomes join through a novel bridge B2a/c where H69 (blue) joins a repositioned h24 (yellow). **f.** H69 and h24 fit into the density at the subunit interface.

Figure 2: Dim1 stabilizes h24 at the 80S-like pre-ribosome interface. a. Local classification followed by refinement and local B-factor sharpening in Relion 3.0 revealed a bi-lobed density at the 60S-pre-40S interface that matches the Dim1 structure (blue). The position of Dim1 in an earlier cytoplasmic pre-40S intermediate (red, Dim1 fit into EMD-4218 (13)) is also shown, demonstrating its repositioning at the interface. **b.** Dim1 modeled into the bi-lobed density at the interface. **c.** Dim1 moves with h24 away from the platform (blue) relative to where they are located in pre-40S ribosomes (red). **d.** Phe231, Arg233, and Lys234 (Dim1-FRK) (orange) face h24. Ile250, Lys253 and Asn254 (Dim1-IKN) (yellow) face Rpl11 in the 60S subunit. **e.** Phe231, Arg233, and Lys234 (orange) and Ile250, Lys253 and Asn254 (yellow) do not face any structural elements in pre-40S subunits. **f.** Dim1-FRK blocks subunit joining. Whole cell extracts from cells depleted of endogenous Dim1 and Fap7 (Gal::Dim1;Gal::Fap7) for 16-20 h and supplemented with plasmids encoding wild type or mutant Dim1 as indicated were fractionated on 10-50% sucrose gradients and the sedimentation of pre-40S ribosomes containing 20S rRNA were probed by Northern blot analysis. 80S-like ribosomes sediment in fractions 6-7 and contain 20S and 25S rRNA. Blocking the formation of 80S-like ribosomes will lead to sedimentation of pre-40S (without 25S rRNA) in fractions 3-5 (4, 5, 37). **g.** Dim1-IKN impairs subunit joining. Dim1 and Fap7 were depleted for 16-20 h and cells were supplemented with plasmids encoding Fap7-K20R (inactive Fap7) and wild type or mutant Dim1 as indicated.

Figure 3: Tsr1 is repositioned to the beak. a. The position of Tsr1 in 80S-like ribosomes (green) is substantially different from the position previously identified in an earlier cytoplasmic pre-40S intermediate (pink), rotated away from the head but still interacting with h44 (purple) (Model from EMD-8349 (11)). **b.** Close-up of the Tsr1 density and atomic model. **c.** Growth of Gal::Tsr1 cells containing plasmids encoding wild type Tsr1, or a truncation lacking the N-terminal helix (Tsr1-□N74) were compared by 10-fold serial dilution on YPD or YPGal plates. **d.** Whole cell extracts from cells in panel c were fractionated on 10-50% sucrose gradients and fractions were probed by Northern blot. **e.** The opened pre-40S and 60S interface leaves space for eIF5B (yellow) across h44 (purple), blocking the early-forming B3 bridge (marked by nucleotides 1655-1657, shown as purple spheres). Model was obtained by superimposition of the 60S subunits from the 80S-like pre-ribosome structure here and the eIF5B-bound mature 80S ribosome (PDB ID 4V8Z (21)). **f.** If subunits were joining in the canonical mature 80S-structure, Tsr1 binding would block eIF5B recruitment. Model was obtained by superimposition of the 40S subunits from the 80S-like pre-ribosome structure here and the eIF5B-bound mature 80S ribosome (PDB ID 4V8Z (21)). The clashscore, as defined in Phenix (36) as the number of overlaps greater than 0.4 Å/1000 atoms, increases from 170 when 60S is superimposed to position eIF5B to 780 when 40S is superimposed to position eIF5B, an increase from 2% to 11% of the total atoms in Tsr1.

Figure 4: The pre-40S platform is opened to allow for Fap7 recruitment. a. After local classification at the platform, alignment, and local B-factor sharpening in Relion3.0, the dominant class has density that corresponds to Rps1 (red), Rps14 (orange), and Pno1 (yellow) albeit not at their final position. **b.** Close-up of the segmented-out platform density. **c.** In 80S-like ribosomes Rps1 (red), Rps14 (orange) and Pno1 (yellow) are shifted outwards relative to their positions in an earlier pre-40S intermediate (PDB ID 6FAI (12), Rps1, Rps14, and Pno1 in gray). **d.** Growth of Gal::Pno1 cells containing an empty vector (e.v.), wild type Pno1, or Pno1-QDF (Q153E; D157R; F237A) (Top) or of ΔRps14B; Gal::Rps14A cells containing an empty vector (e.v.), wild type Rps14, or Rps14-R107E plasmids (Bottom) were compared by 10-fold serial dilution on YPD or YPGal plates. **e.** Whole cell extract from cells depleted of Fap7 and containing wild type Rps14 or Rps14-R107E were fractionated on 10-50% sucrose gradients and fractions were probed by Western blot. Bound Pno1 was calculated as the percent of Pno1 in fractions 4-13 compared to total Pno1. **f.** Whole cell extract from cells depleted of Fap7 and containing wild type Pno1 or Pno1-QDF were fractionated on 10-50% sucrose gradients and fractions were probed by Western blot. Bound Pno1 was calculated as in **e**.

Figure 5: 80S-like ribosomes enable Fap7 recruitment. a. Docking Fap7•Rps14 (Fap7, chain G and Rps14, chain F) from PDB ID 4CW7 (26) onto Rps14 (orange) in 80S-like ribosomes places Fap7 (cyan) in direct contact with Dim1 (blue), as predicted by previous biochemical data (5). **b.** Residues R114, Y116, D118 in Fap7 (Fap7-RYD, shown in orange), R41, V42, M46 (Rps14-RVM, shown in blue) and K49E (shown in purple) in Rps14 are at the interface between Fap7 and Rps14, that is formed between chains G and F). **c.** Growth of Gal::Fap7 (Top) or ΔRps14B; Gal::Rps14A (Bottom) cells containing an empty vector (e.v.), wild type, or mutant proteins were compared by 10-fold serial dilution on YPD or YPGal plates. Fap7-RYD: R114E; Y116A; D118K, Rps14-RVM: R41E; V42L; M46A. **d.** Interface mutations in Fap7 or Rps14 weaken their binding affinity for each other. Shown are Coomassie-stained SDS-PAGE gels of protein binding assays on amylose beads of purified, recombinant MBP-Fap7 or MBP-Fap7-RYD and SUMO-Rps14 or SUMO-Rps14-RVM. In, input; Ft, flow-through; W, final wash; El, elution. **e.** Doubling time, in minutes, of cells depleted of endogenous Dim1 and Fap7 (Gal::Dim1; Gal::Fap7) and transformed with plasmids encoding wild type or Dim1-EKR (E93R; K96D; R97E) and either wild type Fap7 or Fap7-RYD. The white column represents the expected doubling time if there was no rescue of Fap7-RYD by Dim1-EKR (See also (5)). The height of this column was calculated by multiplying the observed fold differences for each single mutation (RYD with EKR). The data are the average of 16-17 biological replicates and the error bars represent SEM. Unpaired t-test was performed comparing expected and actual doubling times of cells expressing Fap7-RYD and Dim1-EKR. *p-value = 0.030. **f**. The Fap7 binding site on Rps14 is blocked by h23 in nucleolar 90S processosomes (6-8), and earlier 40S assembly intermediates (10, 12). Opening of the platform temporarily removes h23, enabling Fap7 recruitment to promote Dim1 release (5).

Figure 1

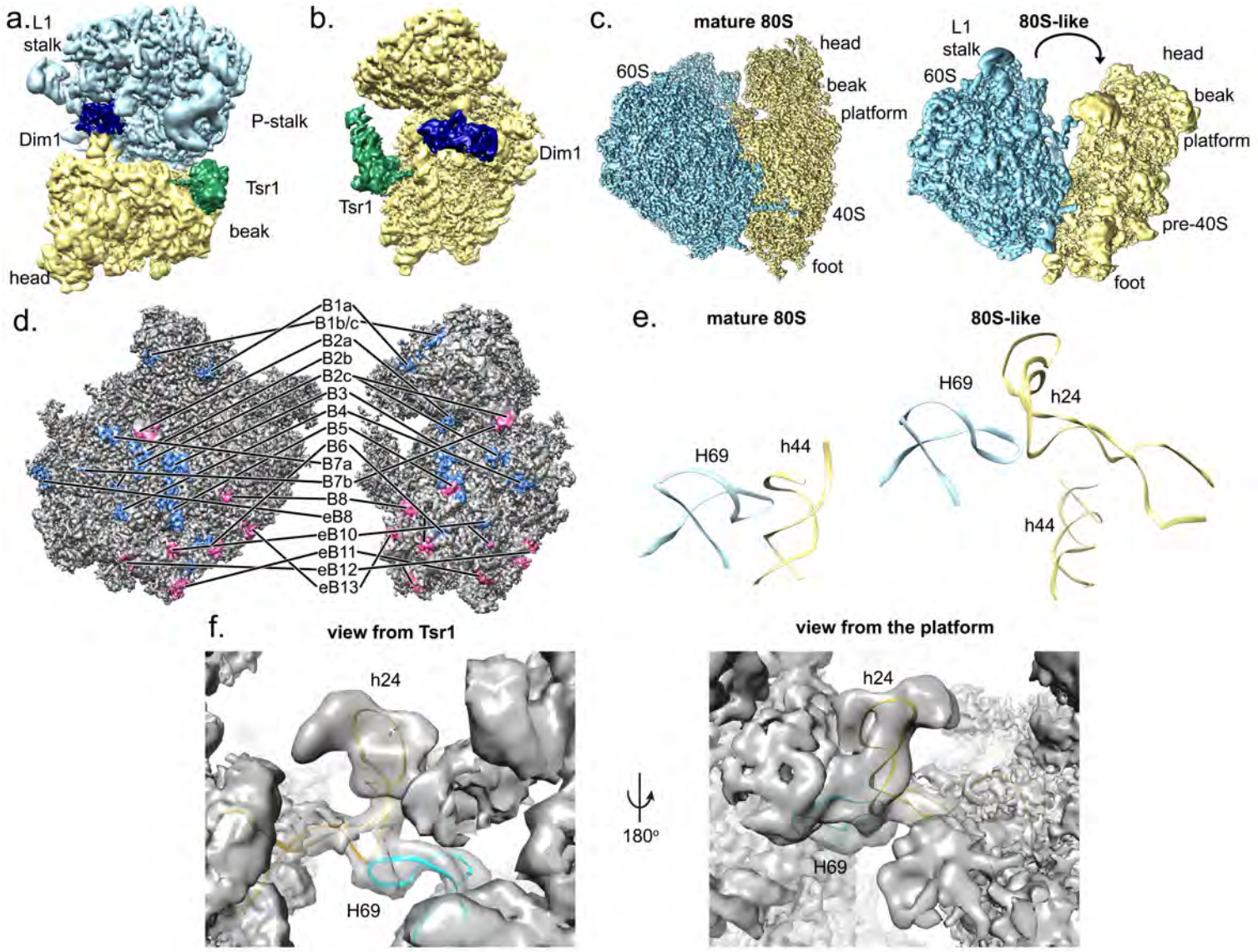
a.
L1 stalk
Dim1
P-stalk
Tsr1
beak
head
b.
Dim1
Tsr1
c.
mature 80S
head
beak
platform
60S
40S
foot
L1 stalk
80S-like
head
60S
beak
platform
pre-40S
foot
d.
B1a
B1b/c
B2a
B2b
B2c
B3
B4
B5
B6
B7a
B7b
B8
eB8
eB10
eB11
eB12
eB13
e.
mature 80S
80S-like
H69
h44
H69
h24
h44
f.
view from Tsr1
h24
H69
180°
view from the platform
h24
H69

Figure 2

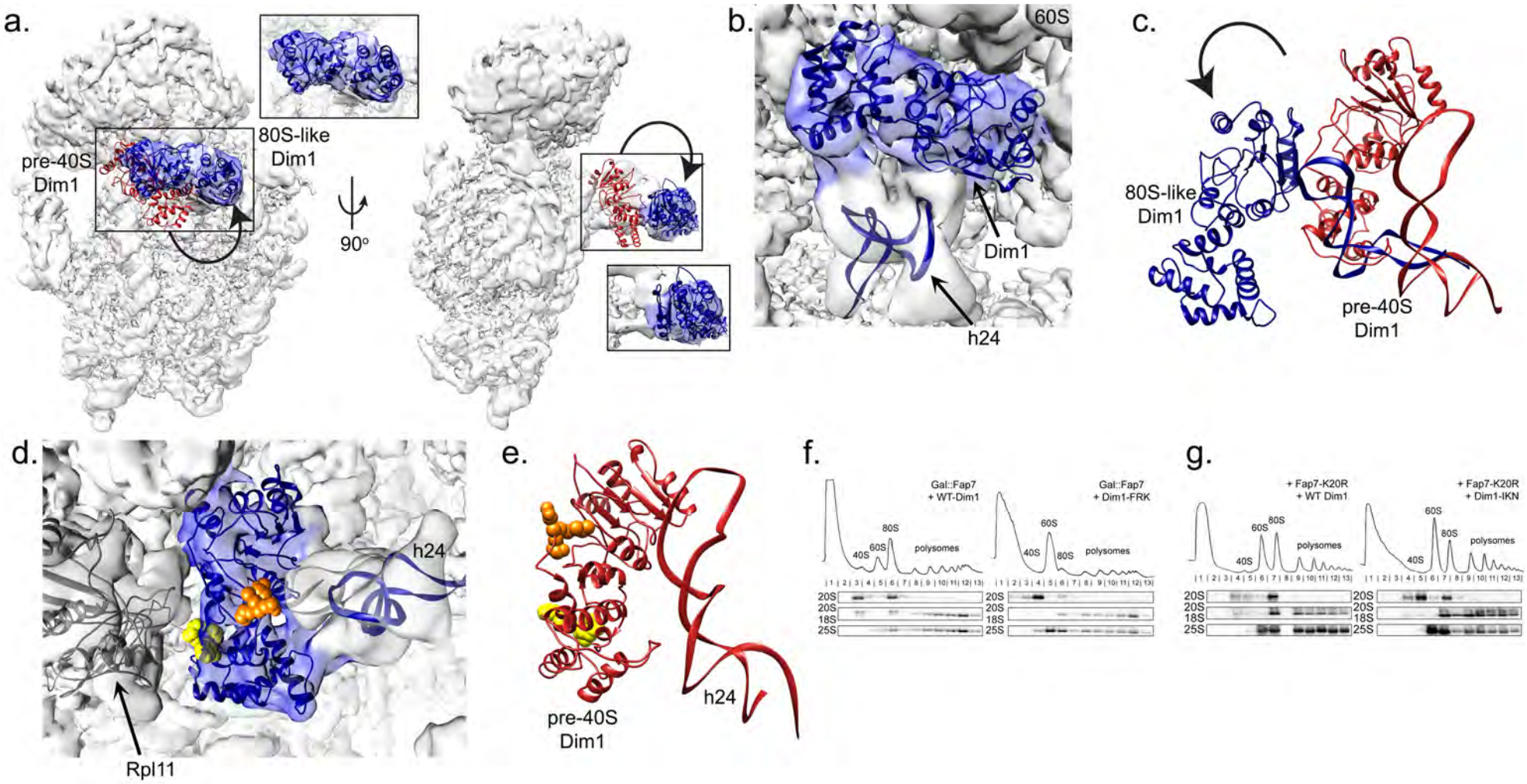
a.
pre-40S
Dim1
80S-like
Dim1
90°
b.
60S
Dim1
h24
c.
80S-like
Dim1
pre-40S
Dim1
d.
h24
Rpl11
e.
pre-40S
Dim1
h24
f.
Gal::Fap7
+ WT-Dim1
Gal::Fap7
+ Dim1-FRK
40S
60S
80S
polysomes
20S
18S
25S
g.
+ Fap7-K20R
+ WT Dim1
+ Fap7-K20R
+ Dim1-IKN

Figure 3

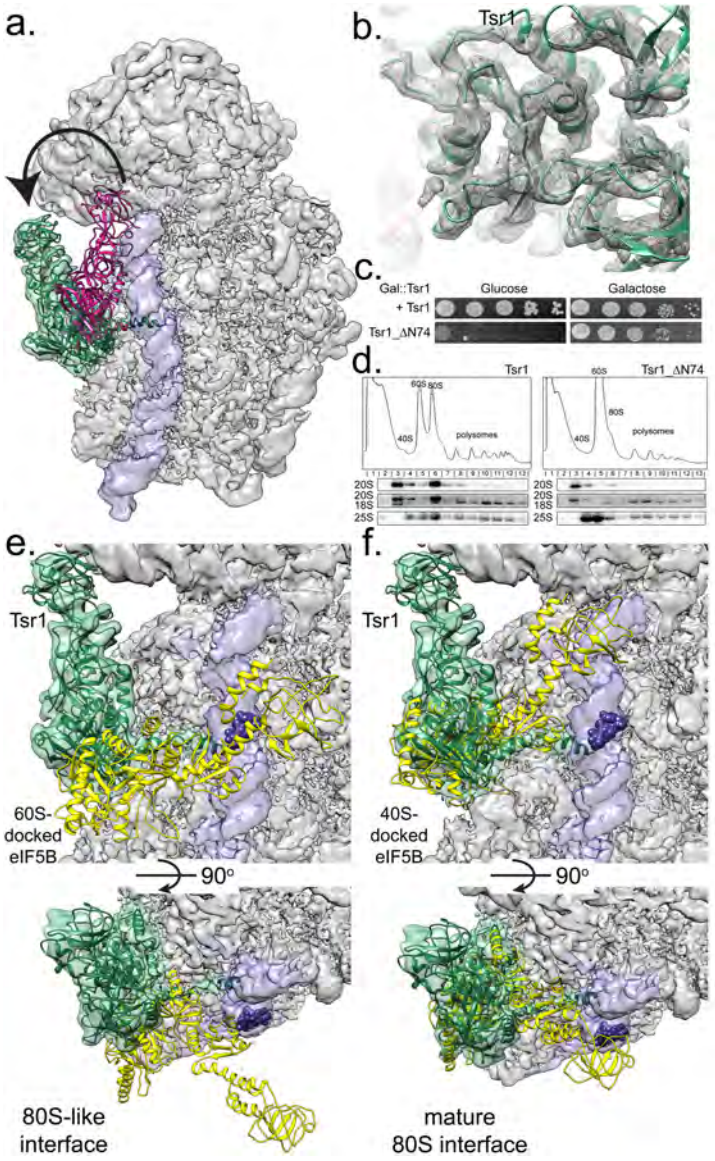
a.
b.
Tsr1
c.
Gal::Tsr1
+ Tsr1
Tsr1_ΔN74
Glucose
Galactose
d.
Tsr1
Tsr1_ΔN74
60S
80S
40S
polysomes
20S
20S
18S
25S
e.
Tsr1
60S-
docked
eIF5B
90°
80S-like
interface
f.
Tsr1
40S-
docked
eIF5B
90°
mature
80S interface

Figure 4

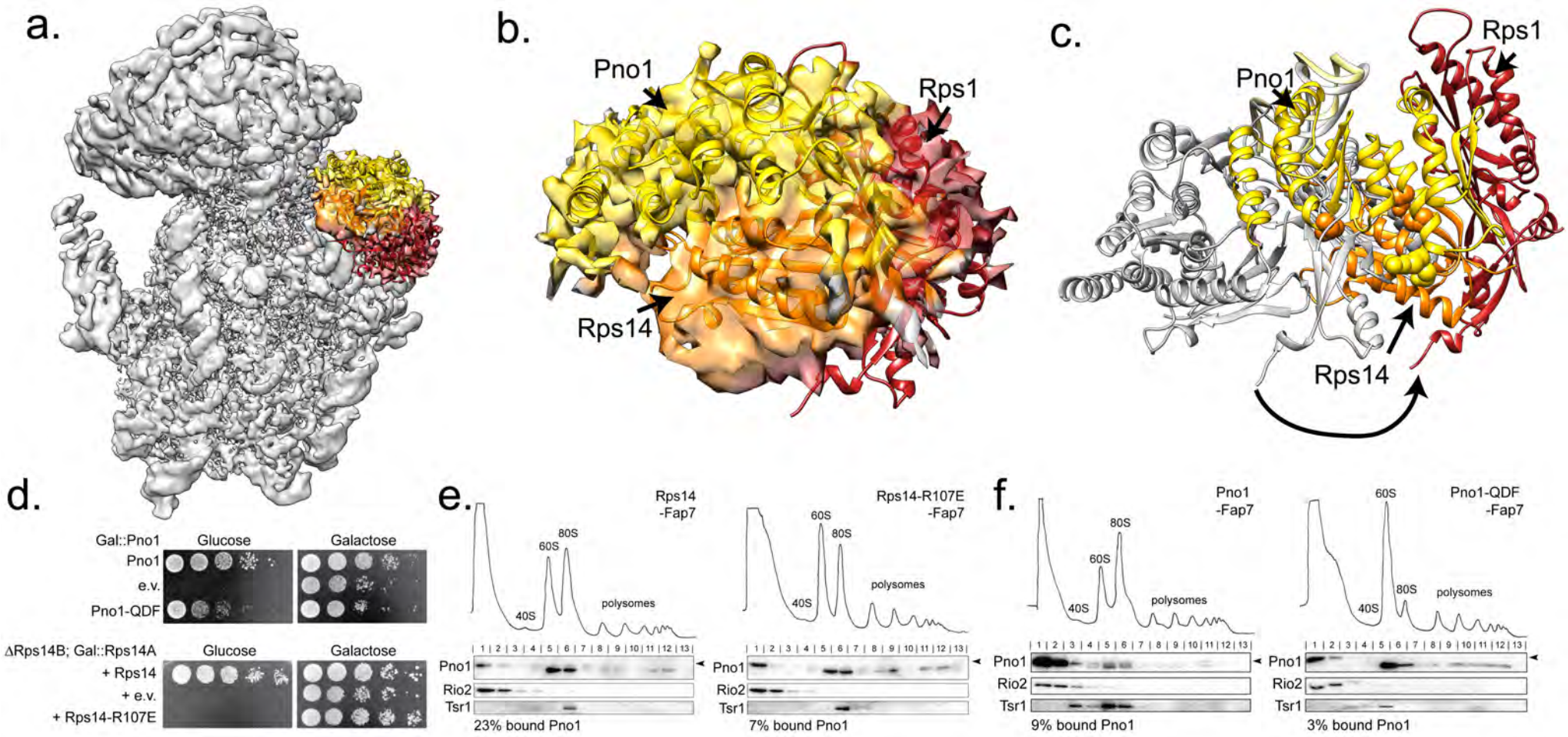
a.
b.
Pno1
Rps1
Rps14
c.
Pno1
Rps1
Rps14
d.
Gal::Pno1
Glucose
Galactose
Pno1
e.v.
Pno1-QDF
ΔRps14B; Gal::Rps14A
Glucose
Galactose
+ Rps14
+ e.v.
+ Rps14-R107E
e.
Rps14
-Fap7
40S
60S
80S
polysomes
Pno1
Rio2
Tsr1
23% bound Pno1
Rps14-R107E
-Fap7
7% bound Pno1
f.
Pno1
-Fap7
9% bound Pno1
Pno1-QDF
-Fap7
3% bound Pno1

Figure 5

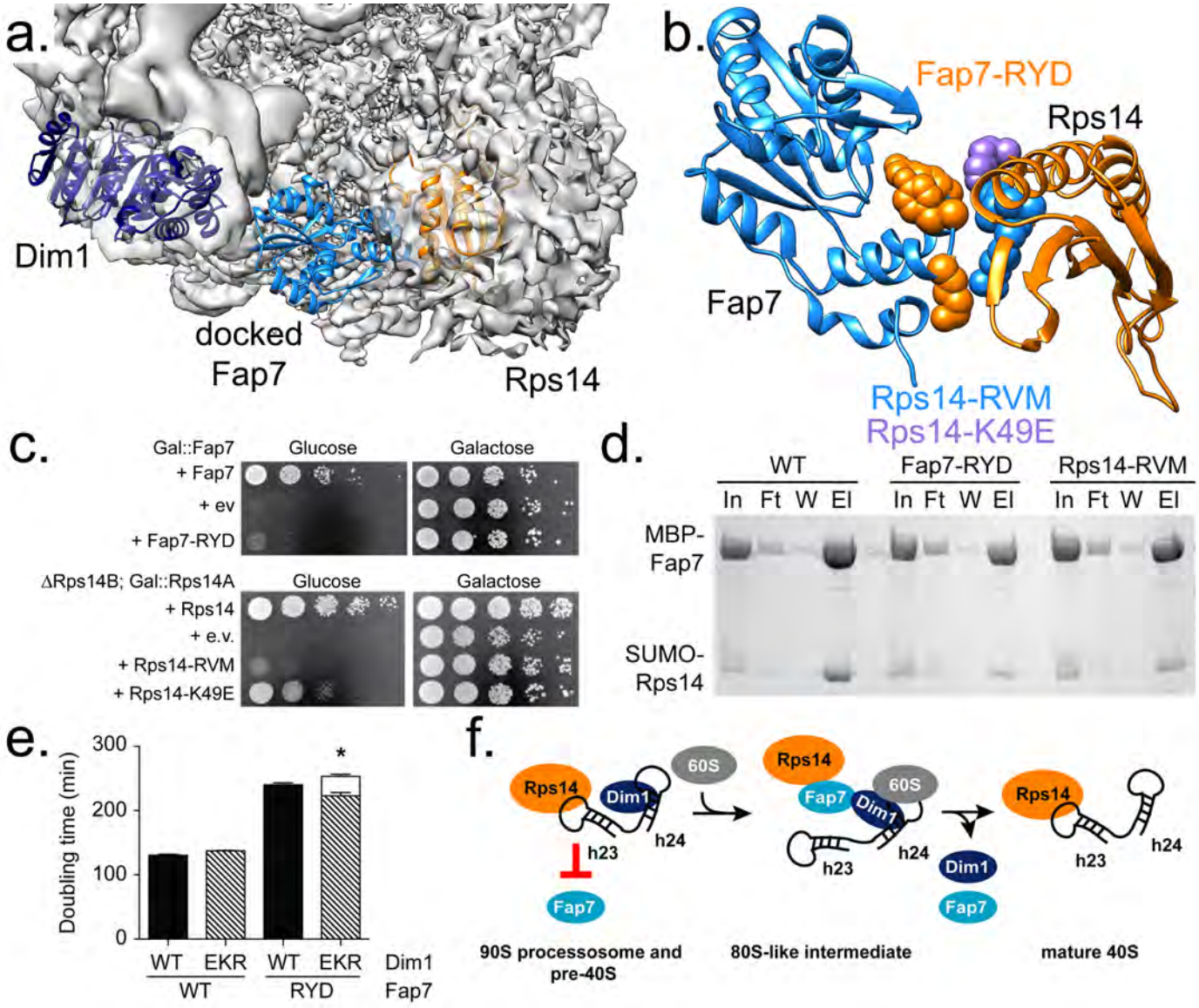
a.
Dim1
docked
Fap7
Rps14
b.
Fap7-RYD
Rps14
Fap7
Rps14-RVM
Rps14-K49E
c.
Gal::Fap7
+ Fap7
+ ev
+ Fap7-RYD
Glucose
Galactose
ΔRps14B; Gal::Rps14A
+ Rps14
+ e.v.
+ Rps14-RVM
+ Rps14-K49E
d.
WT
Fap7-RYD
Rps14-RVM
In Ft W El
MBP-Fap7
SUMO-Rps14
e.
Doubling time (min)
300
200
100
0
*
WT EKR WT EKR Dim1
WT RYD Fap7
f.
Rps14
Dim1
60S
h24
h23
Fap7
90S processosome and pre-40S
80S-like intermediate
mature 40S

Supplementary Materials

Jay Rai[1,2], Melissa D. Parker[2,3], Haina Huang[3], Stefan Choy[3], Homa Ghalei[3,4], Matthew C. Johnson[1,5], Katrin Karbstein[3,6,7] and M. Elizabeth Stroupe[1,7]

[1] Department of Biological Science and the Institute of Molecular Biophysics, Florida State University, Tallahassee, Florida, 32306

[2] these authors contributed equally

[3] Department of Integrative Structural and Computational Biology, The Scripps Research Institute, Jupiter, Florida, 33458

[4] Present address: Emory University School of Medicine, Department of Biochemistry, Atlanta, Georgia

[5] Present address: University of Washington, Department of Biochemistry, 1959 NE Pacific Street, Box 357350, Seattle, WA 98195

[6] HHMI Faculty Scholar

[7] To whom correspondence should be addressed: kkarbst@scripps.edu; mestroupe@bio.fsu.edu

Table 1: Date acquisition parameters

Microscope	Titan Krios
Detector	DE-64
Voltage	300 kV
Electron source	Field Emission Gun
Pixel size (Å/pixel)	1.24
Defocus range (μm)	1.3 -2.5
Nominal Magnification	59000x
Dose rate ($e^-/Å^2$)	25
Frames per exposure	42
Collecting mode	Counting
CTF parameter estimation software	Gctf
Number of micrographs selected for frame alignment	2,129
Framealingment software	MotionCorr 2
Number of particles picked	455,719
Reconstruction software	Relion 3.0
Applied symmetry	C1
Resolution method	FSC 0.143 cut-off
Local resolution determining software	Resmap
EM method	Single-particle
Number of particles contributed in Empty-pre-ribosomes (Resolution) (Applied b-factor during sharpening)	55,949 (3.6 Å) (-114.59)
Number of particles contributed in 80S-like pre-ribosome (Resolution) (Applied b-factor during sharpening	90,692 Small subunit (3.7 Å) (-106.81) Large subunit (3.4 Å) (-100.21)
Model building software	Coot
Model refinement software	Phenix and Coot
Map visualization software	Chimera

Table 2: Refinement and Model quality (pre-40S)

CC (map_model)	0.7
RMSD (Bond lengths)/ (Bond angles)	0.014 Å/1.201˚
Ramachandran plot (%)(Outliers/Allowed/Favored)	0.18/15.61/84.21
Rotamer outliers (%)	0.99
Cβ outliers (%)	0.02
MolProbilty score	2.54
Clash score	23.71
ADP (B-factors) (min/max/mean) Protein Nucleotide	 6.7/102.57/55.76 23.52/186.45/78.3
dFSC model (0.5 cut-off)	3.7 Å
dFSC (half maps; 0.143 cut-off)	3.6 Å

Table 3: Refinement and Model quality (60S)

CC (map_model)	0.9
RMSD (Bond lengths)/ (Bond angles)	0.007 Å/0.703˚
Ramachandran plot (%)(Outliers/Allowed/Favored)	0.17/9.2/90.63
Rotamer outliers (%)	0.07
Cβ outliers (%)	0.00
MolProbilty score	2.13
Clash score	12.18
ADP (B-factors) (min/max/mean) Protein Nucleotide	 104.73/699.66/168.65 110.27/937.53/168.14
dFSC model (0.5 cut-off)	3.5 Å
dFSC (half maps; 0.143 cut-off)	3.4 Å

Table 4: Image processing

CTF parameter estimation software	Gctf
Number of micrographs selected for frame alignment	2,129
Frame alignment software	MotionCorr 2
Number of particles picked	455,719
Reconstruction software	Relion 3.0
Applied symmetry	C1
Resolution method	FSC 0.143 cut-off
Local resolution determining software	Resmap
EM method	Single-particle
Number of particles contributed in Empty-pre-ribosomes (Resolution)	55,949 (3.6 Å)
Number of particles contributed in 80S-like pre-ribosome (Resolution)	90,692 Small subunit (3.7 Å) Large subunit (3.4 Å)
Model building software	Coot
Model refinement software	Phenix and Coot
Map visualization software	Chimera

Supplemental Figure 1 (supplement to Figure 1): Biochemical and image analysis of 80S-like ribosomes. a. SDS-PAGE and Northern blot analysis of the eluate from the IgG bead purification of Tsr1-TAP;Gal::Fap7 cell lysates showing the assembly factor r-protein, and rRNA content of the specimen. Proteins marked with * were identified with mass spectrometry; all others by Western blot analysis. **b.** Work flow of empty and 80S-like pre-ribosome 3D analysis. Each subunit was independently refined and further 3D classified. **c.** Field of view of 80S-like ribosomes**. d.** Initial 2D classification in RELION-3[1] allows sorting the particles into two classes: empty pre-ribosomes and 80S-like pre-ribosomes. **e.** Empty 80S-like ribosomes have fully-formed platforms with Rps1 (red) and Rps14 (orange). **f.** FSC analysis of empty and 80S-like pre-ribosomes, as well as the independently refined subunits of 80S-like pre-ribosomes. **g.** Euler angle distribution analysis shows neither structure has a significant preferred orientation. **h.** High threshold maps, **i.** local b-factor filtering in Relion3.0, and **j.** local resolution analysis in ResMap (2) show that the core of the molecules is more highly ordered than the peripheral regions. **k.** Dim1, h24, and H69 are at lower resolution than the core of the map but were still resolved at better than 10-Å resolution, revealing their secondary structure. **l.** The platform is also at lower resolution than the core of the map but was still resolved at better than 10-Å resolution. Colors are the same as in **k**.

Supplemental Figure 2 (supplement to Figure 1c): Pre-40S movements within 80S-like ribosomes. a. Eigen vector analysis using multi-body refinement in Relion3.0 (3) shows the majority of the variance describing motions of pre-40S and 60S can be described by the first three Eigen vectors. **b.** Movements of pre-40S can be described by rotation relative to 60S for each of the three Eigen vectors. For each Eigen vector 1-3, only the most extreme positions are shown.

Supplemental Figure 3 (supplement to Figure 1c): The pre-40S subunit in 80S-like pre-ribosomes is in a hyper classical state. Viewing the small subunit from the interface after aligning on the large subunit (not shown for simplicity) shows that the consensus position of pre-40S in 80S-like pre-ribosomes (red) is rotated 23º counterclockwise from the rotated position (PDB ID 3J77 (4), gray), measured around an angle formed from the top of the small subunit heads and the feet. This position is further than in the classical position (PDB ID 3J88 (4), green), which is about 5º counter-clockwise from the rotated position.

Supplemental Figure 4 (supplement to Figure 1d): Bridges B5/B8 and B6 are largely conserved in pre-80S-like pre-ribosomes. a. Despite the opened space between 60S and the pre-40S head, bridges at the foot are either pre-positioned or formed in a similar way to how they are in mature ribosomes. The region within the box is enlarged in b. and c. Elements involved in inter-subunit bridges are either conserved (pink) or broken (blue). **b.** Bridges 5, 6, and 8 are formed by L23 (purple) and L24 (teal) and RNA elements from h44. These are largely formed in a similar way as they are in mature ribosomes **c.** but they interact with different regions of h44 to accommodate the opened and hyper-classical subunit orientations (PDB ID 3J77 (4)).

Supplemental Figure 5 (supplemental to Figure 3): In pre-40S subunits from 80S-like pre-ribosomes, Tsr1 rotates away from the AF Rio2-binding site but leaves its N-terminal helix behind h44. a. Despite the large movement, the N-terminal helix remains behind h44. Tsr1 in 80S-like pre-ribosomes is green. Tsr1 in isolated pre-40S is orange and Rio2 is purple, from PDB 6FAI

(5). **b.** Density for Tsr1's N-terminal helix (green) that goes behind h44 (purple density) shows its bend at Ala63.

Supplemental Figure 6 (supplement to Figure 3): Detached Tsr1 can be found in a subclass of pre-40S ribosomes at low occupancy and resolution, which allows close contact with 60S. a. The molecular model of Tsr1 bound to pre-40S as part of 80S-like pre-ribosomes is docked into a low-resolution subclass of cytoplasmic pre-40S with a variably-positioned Tsr1 (6). **b.** In rotating away from pre-40S, Tsr1 makes close contact with the P-stalk of the 60S subunit.

Supplemental Figure 7 (supplement to Figure 3): Asc1 (pink) and Rps10 (yellow) are in their mature position on the solvent-accessible face on the head of pre-40S found in 80S-like pre-ribosomes.

Supplemental Figure 8 (supplement to Figure 3): Neck repositioning in pre-40S within pre-80S ribosomes a. Overview of pre-40S from 80S-like pre-ribosomes. The boxed region is highlighted in b-e. **b-c.** h31 (green is folded in pre-40S found within pre-80S like pre-ribosomes. **d-e.** h31 is not yet folded in earlier pre-40S assembly intermediates (5,7).

Supplemental Figure 9 (supplement to Figure 3): Head movements after folding of h31. The view is the same as in Figure S8. **a.** Comparing pre-40S (blue) to the later 80S-like (gray) head position. **b.** Comparing pre-80S-like (gray) to the classical (blue) head position after superimposition of the bodies. **c.** Comparing pre-80S-like (gray) to the rotated (blue) head position after superimposition of the bodies.

Figure S10 (supplement to Figure 4): Biochemical analysis of Pno1 and Rps14 variants preclude early maturation defects. a. Northern both analysis of total RNA from Gal::Pno1 cells supplemented with an empty vector (e.v.), wild type Pno1, or Pno1-QDF (Q153E;D157R;F237A) (Left). Quantification of the Northern blot measuring 20S accumulation normalized to the U2 signal (Right). Average of three biological replicates and the error bars represent the standard error of the mean. **b.** Northern blot analysis total RNA from ΔRps14B;Gal::Rps14A cells supplemented with an empty vector (e.v.), wild type Rps14, or Rps14-R107E (Left). Quantification of the Northern blot as in **a.** (Right).

Figure S11 (supplement to Figure 5): Rps14•Fap7 have two potential interfaces. a. Fap7 has two interfaces with Rps14, one of which fits into 80S-like ribosomes (blue) and the other of which (cyan) clashes with the rRNA (gray). **b**. The FAP7-RYD (orange balls) variant that causes an Rps14 biding defect corresponds to interface 1, which fits into 80S-like ribosomes. Similarly, the Rps14-RVM (blue balls) and Rps14-K49E (purple balls) variants that cause a Fap7 binding defect also correspond to interface 1. The variants do not fully contribute to interface 2. **c.** The second Fap7-Rps14 interface also clashes in pre-40S ribosomes (Rps14 (orange) and rRNA (gray) from PDB I 6FAI).

Supplemental Movie 1 (supplement to Figure 2): Dim1 movies from its position in the pre-40S to its position in 80S-like ribosomes across the interface.

Supplemental Movie 3 (supplement to Figure 3): Tsr1 moves towards the beak from its position in the pre-40S around a hinge in the N-terminal helix.

Supplementary References

1. J. Zivanov *et al.*, New tools for automated high-resolution cryo-EM structure determination in RELION-3. *Elife* 7, (2018).
2. A. Kucukelbir, F. J. Sigworth, H. D. Tagare, Quantifying the local resolution of cryo-EM density maps. *Nat Methods* 11, 63-65 (2014).
3. T. Nakane, D. Kimanius, E. Lindahl, S. H. Scheres, Characterisation of molecular motions in cryo-EM single-particle data by multi-body refinement in RELION. *Elife* 7, (2018).
4. E. Svidritskiy, A. F. Brilot, C. S. Koh, N. Grigorieff, A. A. Korostelev, Structures of yeast 80S ribosome-tRNA complexes in the rotated and nonrotated conformations. *Structure* 22, 1210-1218 (2014).
5. A. Scaiola *et al.*, Structure of a eukaryotic cytoplasmic pre-40S ribosomal subunit. *Embo J* 37, (2018).
6. Johnson, M. C., Ghalei, H., Doxtader, K. A., Karbstein, K. & Stroupe, M. E. Structural Heterogeneity in Pre-40S Ribosomes. *Structure* 25, 329-340, doi:10.1016/j.str.2016.12.011 (2017).
7. Heuer, A. *et al.* Cryo-EM structure of a late pre-40S ribosomal subunit from Saccharomyces cerevisiae. *Elife* 6, doi:10.7554/eLife.30189 (2017).

Figure S1

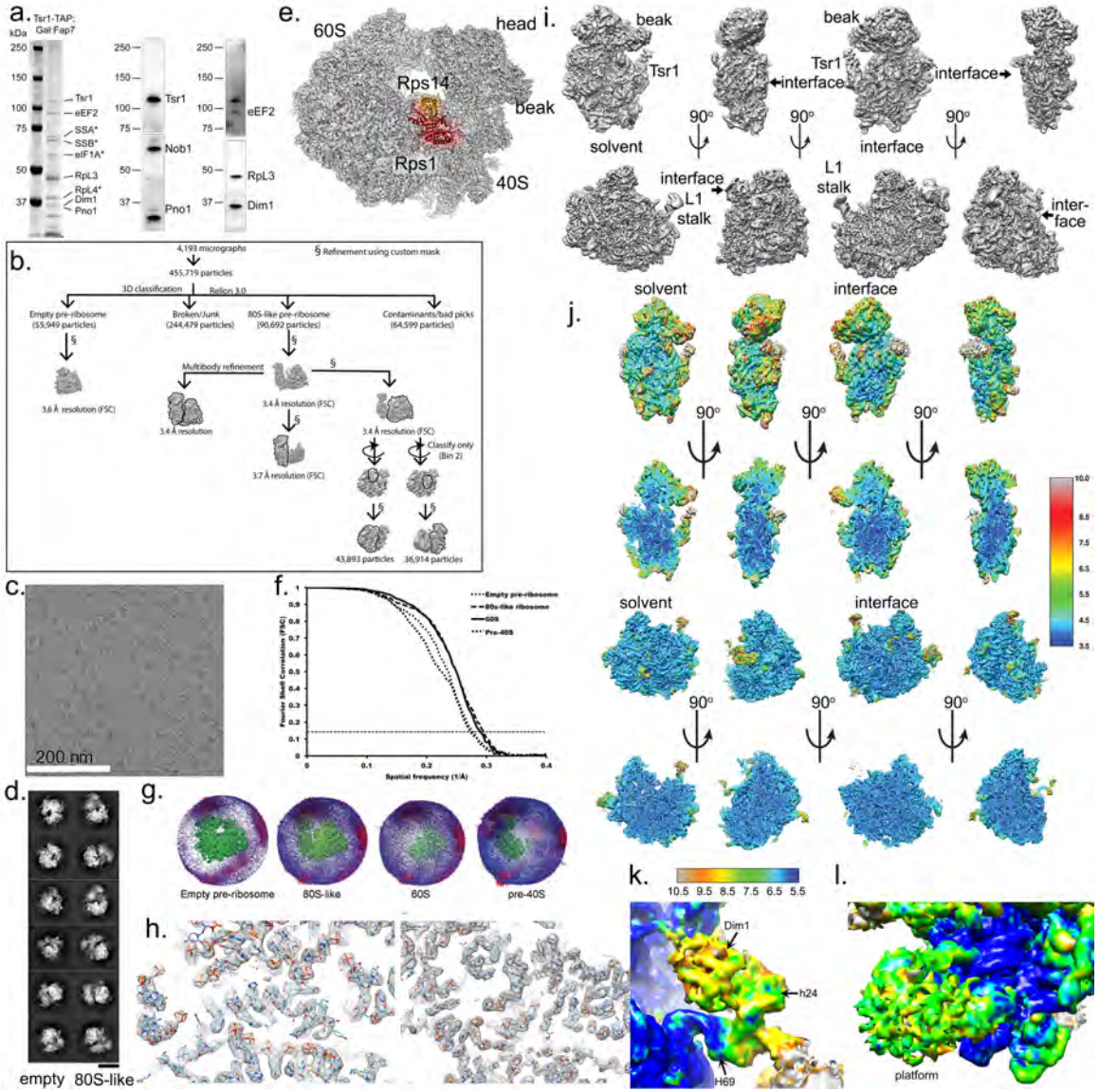
a.
Tsr1-TAP; Gal Fap7
kDa
250
150
100
75
50
37
Tsr1
eEF2
SSA*
SSB*
eIF1A*
RpL3
RpL4*
Dim1
Pno1
Nob1
eEF2
RpL3
Dim1
e.
60S
head
Rps14
beak
Rps1
40S
i.
beak
Tsr1
interface
solvent
90°
L1 stalk
inter-face
b.
4,193 micrographs
§ Refinement using custom mask
455,719 particles
3D classification
Relion 3.0
Empty pre-ribosome (55,949 particles)
Broken/Junk (244,479 particles)
80S-like pre-ribosome (90,692 particles)
Contaminants/bad picks (64,599 particles)
Multibody refinement
3.6 Å resolution (FSC)
3.4 Å resolution
3.4 Å resolution (FSC)
3.7 Å resolution (FSC)
Classify only (Bin 2)
43,893 particles
36,914 particles
j.
solvent
interface
90°
c.
200 nm
f.
Empty pre-ribosome
80s-like ribosome
60S
Pre-40S
Fourier Shell Correlation (FSC)
Spatial frequency (1/Å)
d.
empty
80S-like
g.
Empty pre-ribosome
80S-like
60S
pre-40S
k.
10.5 9.5 8.5 7.5 6.5 5.5
l.
Dim1
h24
H69
platform

Figure S2

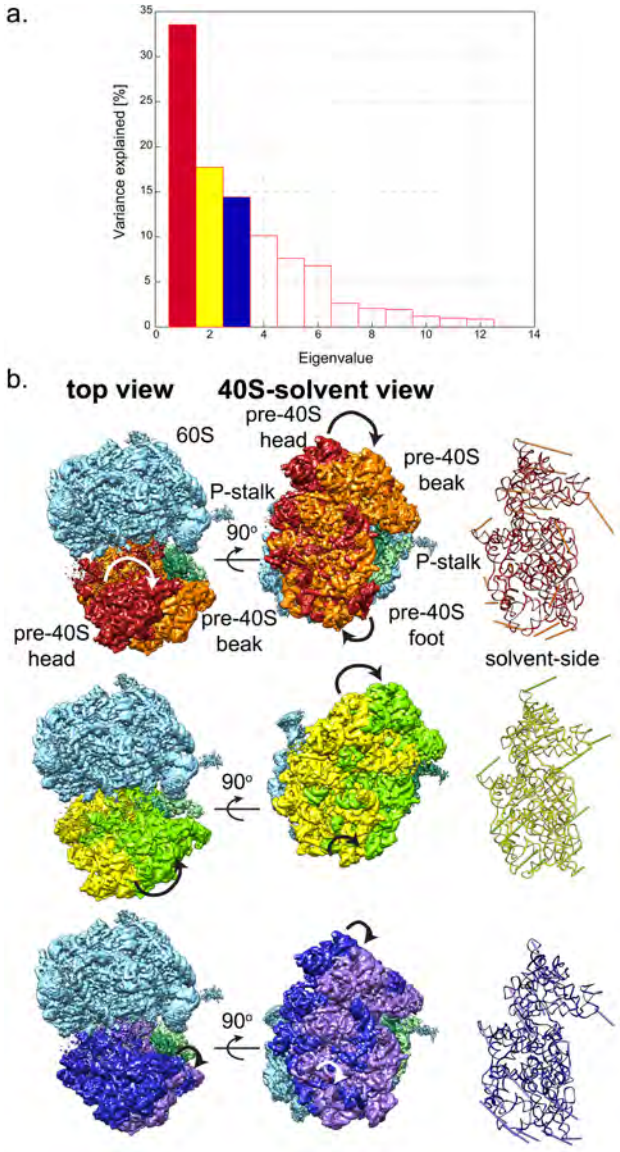
a.
Variance explained [%]
Eigenvalue
b.
top view
40S-solvent view
60S
pre-40S head
pre-40S beak
P-stalk
90°
P-stalk
pre-40S head
pre-40S beak
pre-40S foot
solvent-side
90°
90°

Figure S3

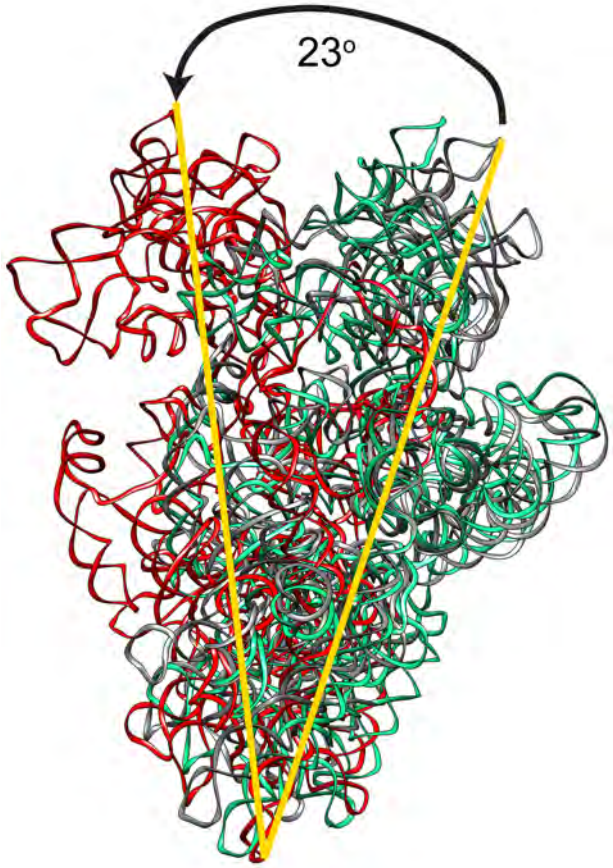

Figure S4

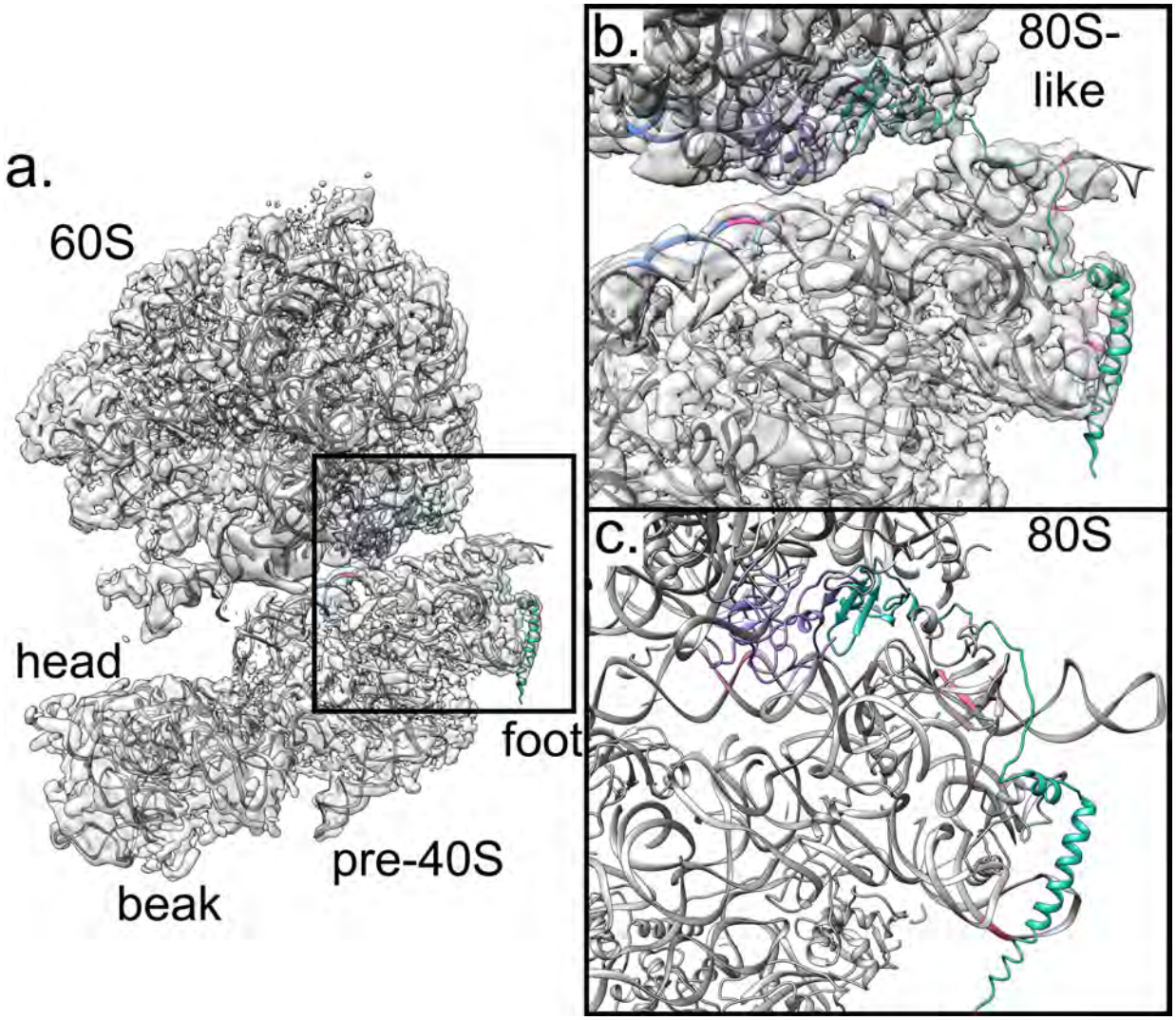

Figure S5

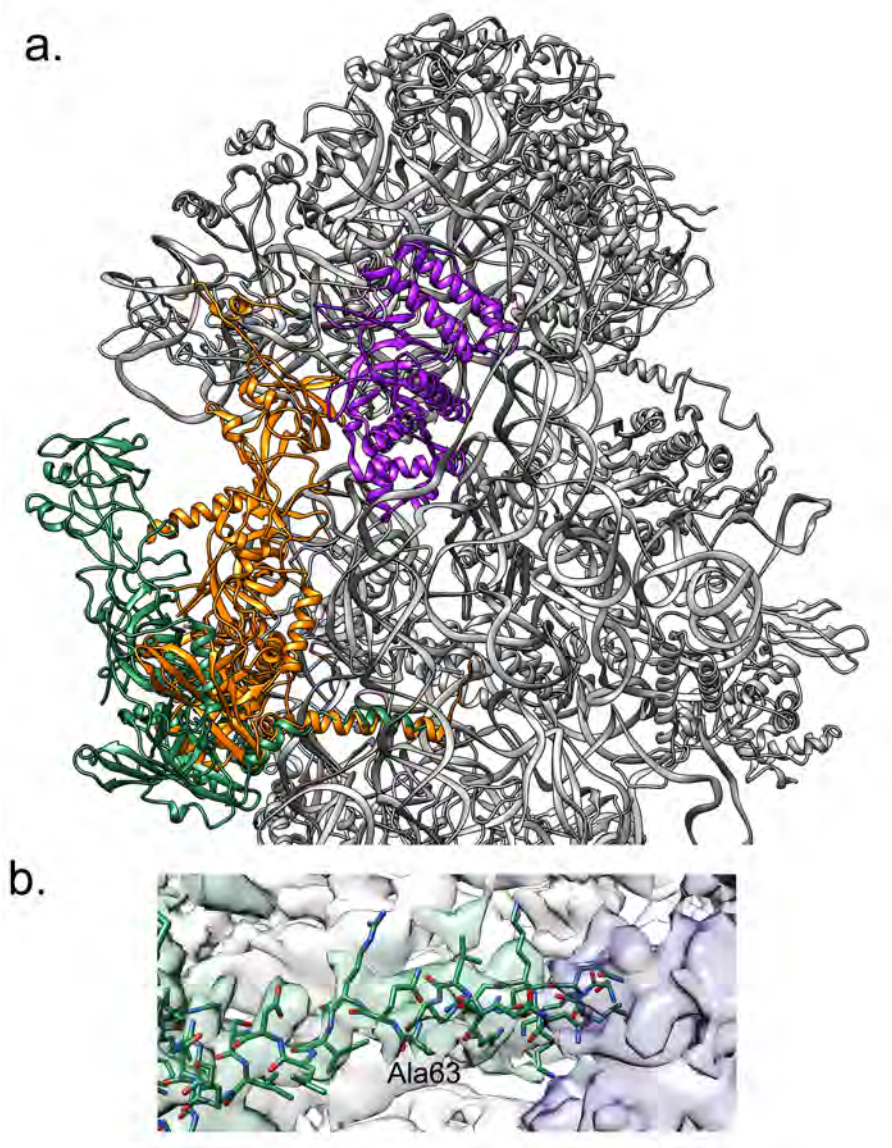

Figure S6

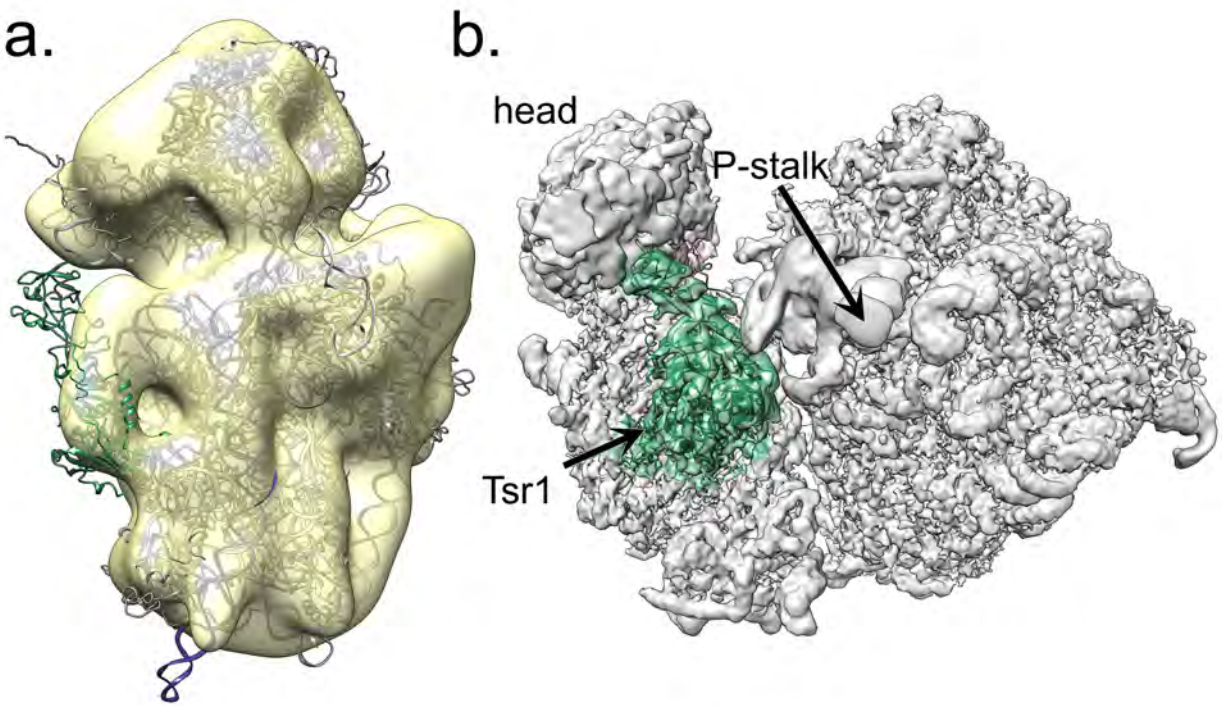

Figure S7

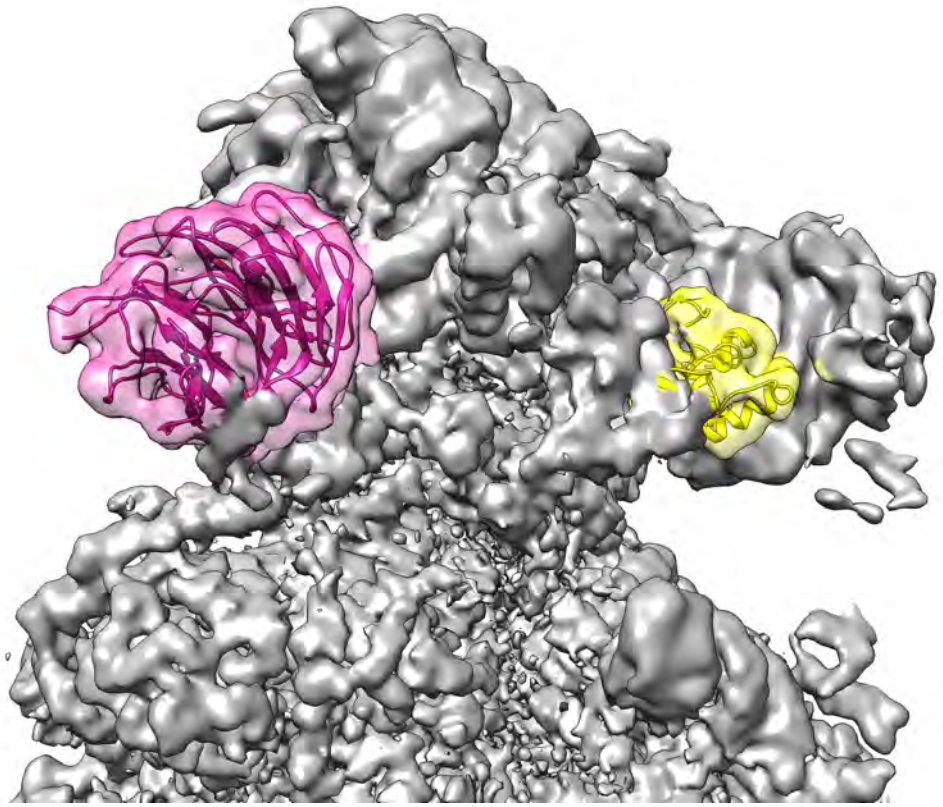

Figure S8

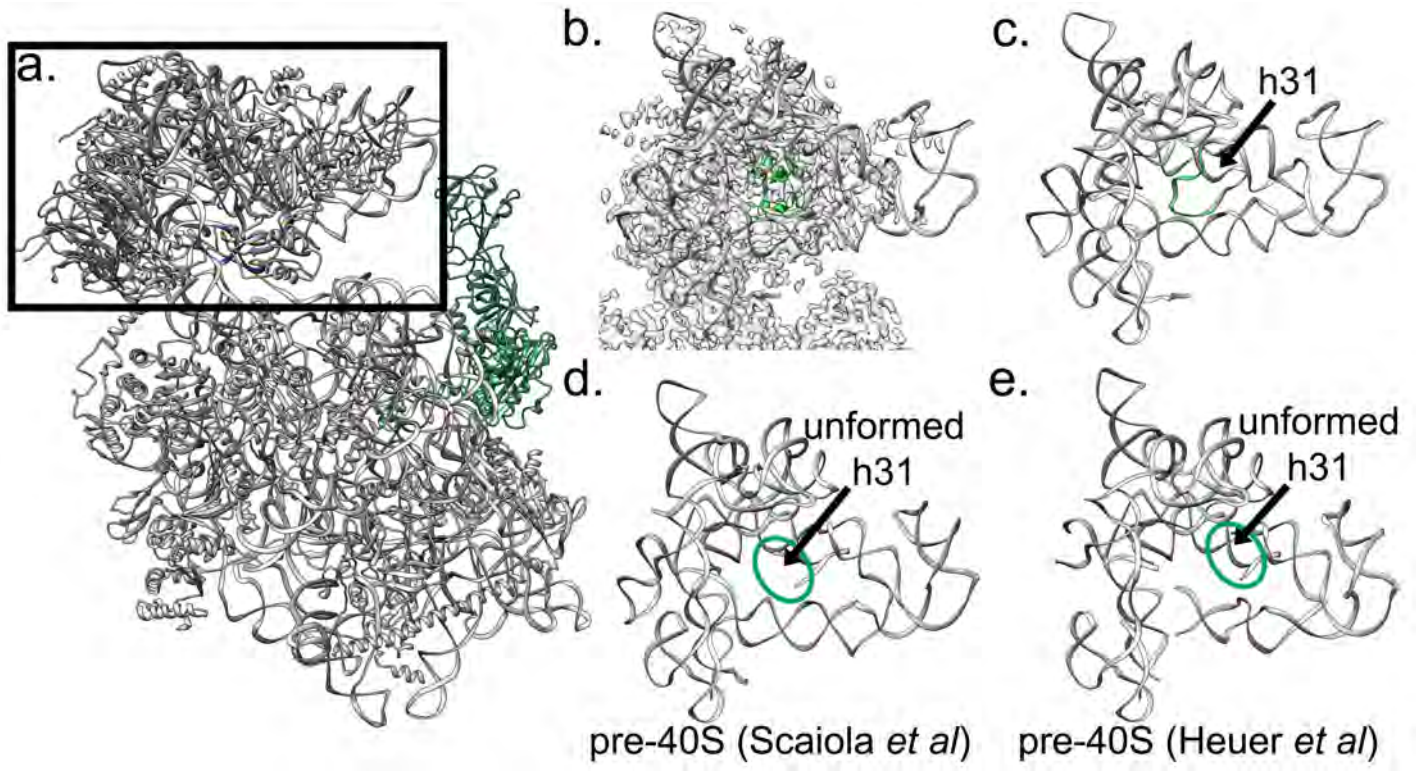
a.
b.
c.
h31
d.
unformed
h31
e.
unformed
h31
pre-40S (Scaiola *et al*)
pre-40S (Heuer *et al*)

Figure S9

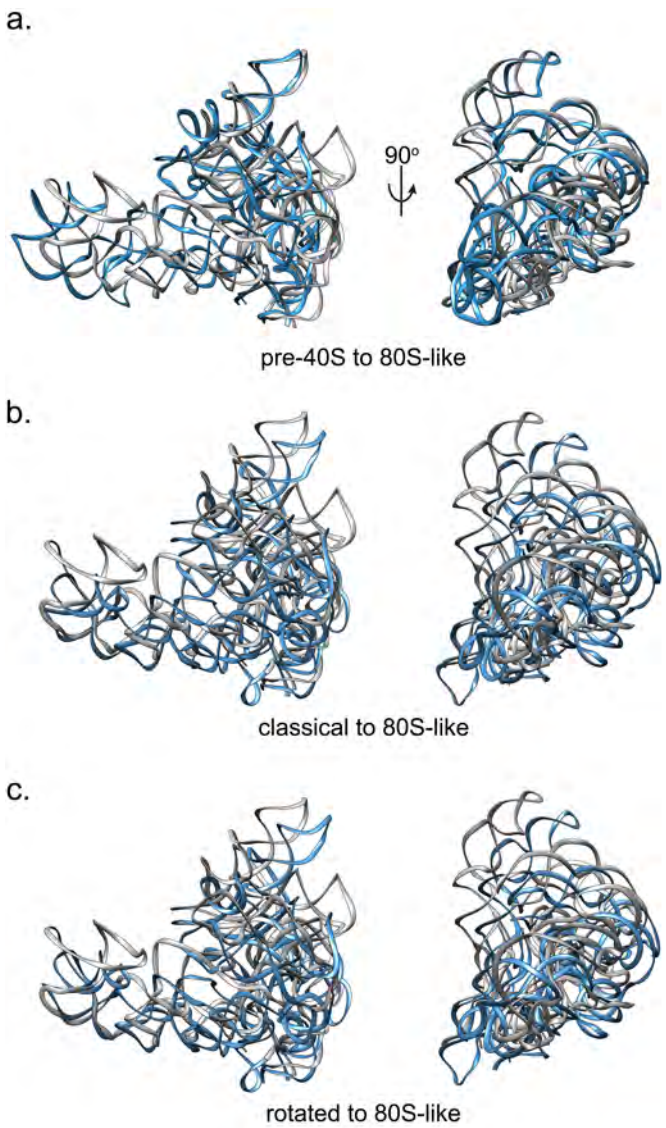
a.
90°
pre-40S to 80S-like
b.
classical to 80S-like
c.
rotated to 80S-like

Figure S10

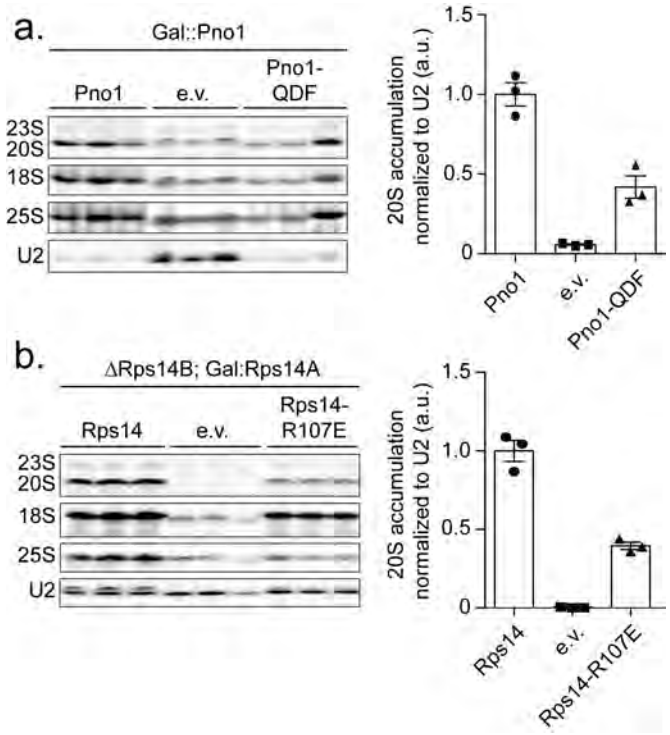
a.
Gal::Pno1
Pno1
e.v.
Pno1-QDF
23S
20S
18S
25S
U2
20S accumulation normalized to U2 (a.u.)
1.5
1.0
0.5
0
Pno1
e.v.
Pno1-QDF
b.
ΔRps14B; Gal:Rps14A
Rps14
e.v.
Rps14-R107E
23S
20S
18S
25S
U2
20S accumulation normalized to U2 (a.u.)
1.5
1.0
0.5
0
Rps14
e.v.
Rps14-R107E

Figure S11

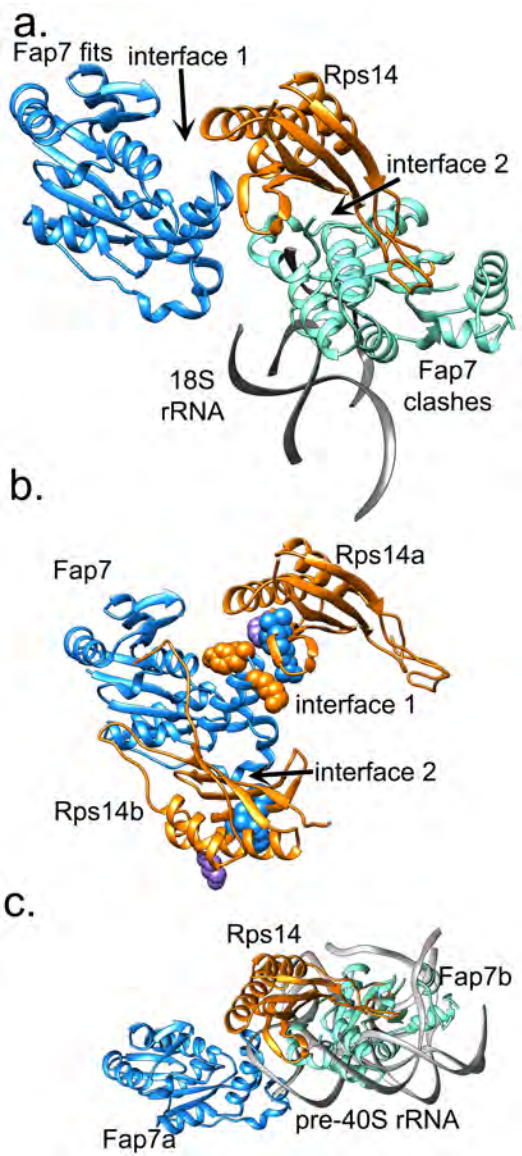
a.
Fap7 fits
interface 1
Rps14
interface 2
18S
rRNA
Fap7
clashes
b.
Fap7
Rps14a
interface 1
interface 2
Rps14b
c.
Rps14
Fap7b
pre-40S rRNA
Fap7a